Journal of Macromolecular Science, Part A
Publication details, including instructions for authors and subscription information:
http://www.informaworld.com/smpp/title~content=t713597274

Influence of RF-Cold Plasma Treatment on the Surface Properties of Paper

F. Denes[a]; Z. Q. Hua[a]; E. Barrios[a]; R. A. Young[a]; J. Evans[b]
[a] Department of Forestry and the Engineering Research Center for Plasma-Aided Manufacturing, University of Wisconsin, Madison, Wisconsin [b] Bureau of Engraving and Printing, Washington, D.C.

To cite this Article Denes, F. , Hua, Z. Q. , Barrios, E. , Young, R. A. and Evans, J.(1995) 'Influence of RF-Cold Plasma Treatment on the Surface Properties of Paper', Journal of Macromolecular Science, Part A, 32: 8, 1405 — 1443
To link to this Article: DOI: 10.1080/10601329508013689
URL: http://dx.doi.org/10.1080/10601329508013689

J.M.S.—PURE APPL. CHEM., A32(8&9), pp. 1405–1443 (1995)

INFLUENCE OF RF-COLD PLASMA TREATMENT ON THE SURFACE PROPERTIES OF PAPER

F. DENES,* Z. Q. HUA, E. BARRIOS, and R. A. YOUNG

Department of Forestry and the Engineering Research Center for Plasma-Aided Manufacturing
University of Wisconsin
Madison, Wisconsin 53706

J. EVANS

Bureau of Engraving and Printing
Washington, D.C.

ABSTRACT

Unprinted, unsized, and sized security papers (SP) were treated under $SiCl_4$-, O_2-, and CF_4-cold plasma conditions. The plasma treatments were carried out in a stainless steel, parallel plate RF (30 kHz) reactor. The influence of plasma parameters, such as RF power, pressure, and treatment time, on the surface properties of plasma-modified security paper was examined. The newly gained surface characteristics were evaluated by Wilhelmy wettability measurements, x-ray photoelectron spectroscopy (ESCA), and scanning electron microscopy (SEM). Statistical experimental designs were used to understand the interactive effects of the plasma parameters. It was found that short treatment times and low RF power values produced the highest wettability with both $SiCl_4$ and O_2 plasmas regardless of the sizing. Printing and durability characteristics of the plasma-treated substrates were equivalent or superior to the standard samples. Mechanisms of plasma-induced surface modifications are discussed for the paper substrates.

INTRODUCTION

Security paper is repeatedly exposed to environmental and handling stress which reduces life expectancy. Mechanical stress, moisture, and dust, as well as UV radiation, affect the service life. Mechanical failure of the substrate (unprinted and unsized paper) erosion of the sizing layer, and ink desorption due to poor surface adhesion are controlled both by kinetic and thermodynamic factors.

The intaglio method is commonly used for printing of various security documents. While printing, if the alkyd ink dries too fast before good wetting can be achieved, poor adhesion will result. Both wetting and adhesion characteristics are controlled by acid–base interactions and morphologies at the interfaces.

The surface chemistry of papers varies both with grade and origin. Different types of surface treatments also modify the surface polarities. The physicochemical nature of the paper, sizing materials, and the inks must be understood and controlled in order to achieve the required printing characteristics.

Most sizing materials for surface treatment of paper are polymeric in nature, composed of large linear macromolecules that have the required characteristics (strength, flexibility, etc.) for an adequate coating. Competition between adhesion and cohesion interactions will control the adhesion efficiency. Mass transfer processes, such as adhesive penetration into the substrate structure and subsequent migration to the surface, can create additional problems. The shapes and the sizes of the pores in the paper, their wettability and swelling characteristics, and the viscosities and surface tension values of the sizing materials eventually control these interactions.

Physicochemical properties of paper and lignocellulosic surfaces have been extensively investigated in the past; however, many aspects which affect surface characteristics have not yet been clarified. Gardner and coworkers [1] used dynamic contact angle (DCA) analysis to study the wettability of different origin wood samples. It was established that the elemental and chemical composition, surface roughness, capillary-flow characteristics, sample storage conditions, and testing speed during DCA measurements have a significant influence on the wettability data. The authors emphasized that combined DCA and x-ray photoelectron spectroscopy (ESCA) represent an adequate tool for evaluation of surface energetics and chemistry of wood.

Wetting properties of cellulose and wood-hemicellulose in the form of films were examined by Luner and coworkers [2] by measurement of critical surface tension of wetting (Zisman's parameter). It was established that the origin of the cellulose, the method of film preparation, and the morphology of the film surfaces influenced the wettability of the samples. The small hysteresis effects observed for the hemicellulose samples were attributed to the presence of energetically uniform surfaces. It was also found that the interaction of cellulose with various fluids ranging from water to nonpolar liquids involves, in addition to hydrogen bonding, strong dispersion forces.

The complex nature of dynamic wettability properties of wood pulp fibers has been investigated by Young [3, 4] and Hodgson and Berg [5] by the Wilhelmy technique. It was found that the water wettability of these fibers is significantly influenced by the varying surface chemistry. When pulps are subjected to elevated temperatures, the presence of residual extractives can have a significant effect on the fiber wettability. These authors emphasized that the wetting properties of single

wood fibers is a critical factor in determining liquid absorption performance of bulk structures composed of the fibers.

Borch and coworkers [6] examined the effect of surface sizing of paper on adhesion to synthetic thermoplastic polymers. It was found that adequate bond strength must be created between the paper and polymer surfaces for achieving proper performance characteristics. Triantafillopoulos and coworkers [7] and Etzler et al. [8] analyzed surface energetics and acid-base chemistry in terms of printability. Etzler and coworkers [8] found that commonly used alkyd varnishes present poor wetting on typically used papers due to the presence of repulsive Lewis acid-base interactions at the interfaces. Slow macromolecular events also contribute to reduced wetting properties. The importance of variations in paper surface chemistry on printability was emphasized.

The shortcomings of paper surface chemistry due to the variable origin and preparation techniques are overcome by use of sizes which uniformly modify the surface characteristics of the paper substrates. Conventional processes offer solutions only through chemical modifications which alter both the surface layers and the base structure and through formulation and application of sizes. Use of sizes for surface modification requires additional expensive processing steps.

Cold plasma chemistry offers unique solutions to this problem since a large spectrum of different types of surface functionalization can be achieved without altering the bulk properties of the materials, even for the most inert polymeric substrates. The active species of a cold plasma (electrons, ions of either polarity, atoms and molecules at various excitation levels, and photons) have sufficient energy (0–20 eV) to dissociate the chemical bonds from all organic-, organometallic-, or elemental-organic structures. Molecular fragments resulting from the gaseous phase plasma reactions interact with the surfaces in the plasma and induce surface functionalization and/or plasma-polymer-based coating processes.

Plasma-surface modification and polymerizations of synthetic materials have been described in the literature [9–16]. Less data are available, however, on plasma-induced surface modification and/or grafting of natural polymers and their technological end-products (textile fibers, cellulose-based films, papers, etc.). Pavlath and coworkers [17–20] studied the effects of various gas discharges on the properties of wool fibers. They found that the plasma treatments resulted in both increased yarn and fabric strength, and increased abrasion and shrinkage resistance. A laboratory-scale continuous flow plasma reactor was also designed and developed in this work to allow fiber processing under low pressure conditions.

A comparative study of O_2, N_2, H_2, Ar, CO, CH_4, and CF_4 plasma-treated cellulosics (linen, cotton, and rayon fibers) and wool, silk, and synthetic fibers (nylon 6 and polyethylene terephthalate) was carried out by Wakida and coworkers [21]. The relative free-radical intensities of irradiated samples were estimated, and it was established that the nature of the plasma gases, the plasma parameters, and the nature of the substrates have a significant influence on the free-radical intensities. Surface coating of cellulosic materials with plasma polymers has also been investigated [22–25]. Improved compatibility with thermoplastic polymers and controlled surface porosity characteristics were reported.

The objective of this work was to modify the surfaces and improve ink adhesion to both unsized and sized security paper through treatment with reactive plasma gases. In this paper, experimental results from a systematic study on surface functionalization of unsized and sized security paper samples under $SiCl_4$, O_2, and CF_4

RF-cold-plasma conditions are described and the newly gained surface properties are discussed.

EXPERIMENTAL

Materials

Sized and unsized security paper samples (160 × 67 mm) were used as received. High purity $SiCl_4$ (Aldrich), O_2, (Liquid Carbonic) and CF_4 (Aldrich) gases were used as plasma media. The $SiCl_4$ was handled in a glove box under an argon blanket. Argon (Liquid Carbonic) was employed as a cleaning agent both in the presence and absence of a plasma. For wetting measurements, methylene iodide from Aldrich Chemical Co. was employed for estimating the dispersive force contribution (nonself-associating probe liquid for dispersive contribution to the surface energy; surface tension 50.8 dyn/cm). Formamide (basic probe liquid for acid-base contribution; surface tension 58.3 dyn/cm) and ethylene glycol (acidic probe liquid for acid-base contribution; surface tension 48.3 dyn/cm) from Aldrich Chemical Co. were used for evaluating polar force values. All Aldrich chemicals were used as received.

Methods

Surface atomic composition of untreated and plasma-treated paper surfaces was analyzed using x-ray photoelectron spectroscopy (ESCA-Perkin Elmer Physical Electronics O 5400 Small Area System; Mg source; 15 kV; pass energy 89.45 eV; angle 45°). The ESCA measurements involved the determination of carbon (C1s), oxygen (O1s), fluorine (F1s,), and silicon (Si2p). All samples were stored under dessicator conditions until the measurements were started in order to avoid moisture-induced surface modifications.

The morphology of virgin and plasma-modified paper surfaces was investigated by scanning electron microscopy (SEM-JEOL JSM-35°C; electron beam accelerating voltage 15 kV; electron gun-target distance 39 mm; vacuum 10^{-6} torr). Gold-coated surfaces were used in all of the experiments.

Contact angle estimations and surface energy component evaluations were carried out using a CAHN Dynamic Contact Angle Analyzer (elevator speed 150 μm/s, humidity 52%; temperature 24°C). Water was employed in all of the cases for contact angle measurements, and formamide (Lewis base) and ethylene glycol (Lewis acid) for acid/base work of adhesion estimations. Methylene iodide was selected for the evaluation of the dispersive force components. The determinations were carried out on vertically positioned 4 × 40 mm paper strip samples in both advancing and receding testing modes.

The plasma-induced molecular fragmentation of $SiCl_4$ was simulated by the low energy-electron MS (LEE-MS) technique (GC-Carlo Erba Fractovap 4162; MS Kratos 25; experimental conditions: column-fused silica; length 30 m; i.d. 0.32 mm; coating 0.25 μm of 5% phenyl and 95% vinyl polysiloxane; injector splitter temperature 25°C; temperature profile of the column: 5 minutes at room temperature then heated up to 250°C at 15°C/min; electron energy 25, 50, and 70 eV). The

MS instrument is a double focusing mass spectrometer (electrostatic analyzer and magnet) provided with an electron impact ion source.

Central composite statistical designs were employed to study the influence of $SiCl_4$, O_2, and CF_4 plasmas on the surface properties of the paper. Pressure in the presence of plasma, RF-power dissipated to the electrodes, and treatment time represented the controlled experimental parameters, and the corresponding water contact angle values of the paper gave comparative information on the wettability characteristics of treated and untreated paper samples.

Due to the high reactivity of Si—Cl bonds in the presence of moisture (Si—Cl functionalities generate Si—OH groups under open laboratory conditions), the influence of plasma parameters on surface atomic composition and its interdependence with wettability characteristics have been analyzed for the treated paper samples. Oxygen and carbon tetrafluoride plasmas lead to higher oxygen and fluorine surface atomic compositions, respectively; their influence on the contact angle values is less complex.

Experimental conditions and constraints (eight different samples treated in 1 day) limited the statistical design to a three-block system. The first two blocks consisted of a full 2^3 factorial design, while the third block represented the axial part of the central composite design. Two identical samples were treated in the center of the experimental region of each block, permitting in this way a test of the reproductibility and repeatability of the experiments and a way to adjust the estimation effects determined by the daily variation in the plasma reactor performance.

Response surface methodology [26] was used to compare the influence of each controlled parameter on the contact angle modifications of the plasma-treated samples. A second-order polynomial was selected to approximate the power-, pressure- and treatment time-dependent contact angle values for $SiCl_4$. For O_2 and CF_4, first-order polynomials with interaction terms were appropriated.

Plasma Treatments

The plasma treatment experiments were carried out in a parallel plate stainless steel cylindrical reactor (Fig. 1) with an electrode diameter of 20 cm and a distance between electrodes of 3 cm. The upper electrode (15) is connected to the matching network and to the RF power supply (30 KHz), and the lower electrode (22) is grounded. The substrates were placed directly on the lower electrode which was provided with a heating element (17) in order to facilitate the removal of possible higher volatility contaminants from earlier experiments during cleaning operations.

The reactor is equipped with two vacuum lines. The high capacity vacuum system is connected by means of 1 inch stainless steel tubing (24) to the reaction chamber and positioned through the center of the lower electrode. This geometry and the gas feeding system composed of a gas chamber (12) and gas inlet orifices dispersed circularly around the upper electrode (10, 14) permitted a symmetrical penetration of the gas flow into the discharge zone located between the electrodes.

The vacuum line is composed of large cross-section valve (25), liquid nitrogen trap (26) and high capacity mechanical vacuum pump (29), and it assures quick evacuation of the system to the base pressure level and protection of the pump from chemical contamination. The high surface area of the trap also excludes pump oil flashback during the experiments. The second vacuum line (low capacity) is directly

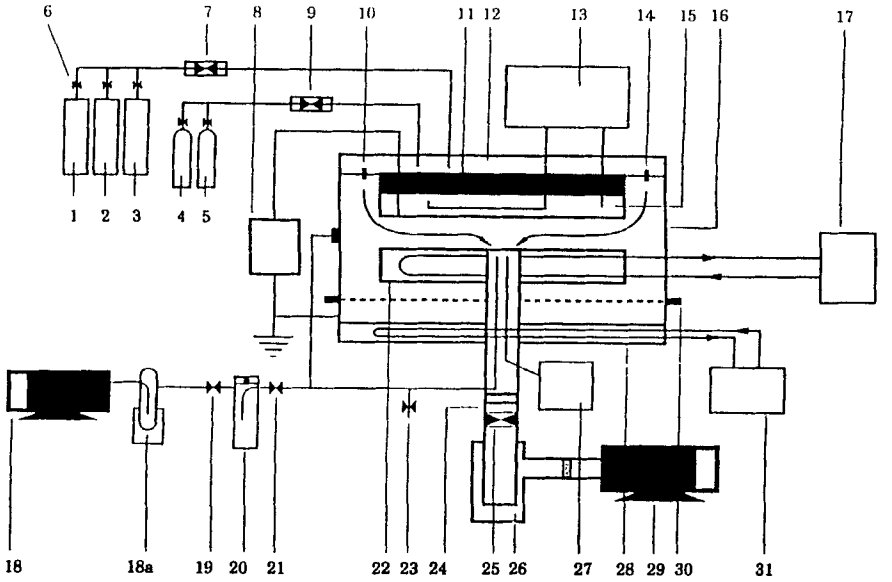

FIG. 1. Capacitively-coupled stainless steel RF-plasma reactor. Parallel plate RF cold plasma installation. 1, 2, 3: Gas and $SiCl_4$ reservoirs. 4: Argon reservoir. 5: Monomer reservoir. 6, 19, 21, 23: Stainless steel needle valves. 8: HF generator. 7, 9: Flow controller. 10, 14: Monomer and/or gas inlet orifices, located circularly around the upper electrode (shower-type feeding). 11: Electric insulator disc. 12: Gas mising chamber. 13: Programmable refrigerated circulator. 15: Drum-type stainless steel upper electrode. 16: Cylindrically shaped upper part of reactor. 17: Temperature controller for the built-in electric heater of the lower electrode. 18: Mechanical vacuum pump. 20: Stainless steel liquid nitrogen trap for collecting the plasma-generated molecular mixture. 22: Grounded lower stainless steel electrode. 24: One-inch diameter stainless steel connecting tubing. 25: Large cross section butterfly-type valve. 26: Stainless steel liquid nitrogen trap for protecting vacuum pump. 27: Vacuum gauge. 28: Drum-type stainless steel lower part of the reactor. 29: High capacity mechanical vacuum pump. 30: Rubber O-ring mediated circular vacuum tight sealing. 31: Refrigerated recirculator.

connected to the reaction chamber through 5 mm stainless steel tubing and a removable leakproof connection and allows direct sample extraction from the discharge zone. It is composed of stainless steel needle valves (19, 21, 23), a specially designed stainless steel liquid nitrogen trap (20) provided with a vacuum-tight removable cap and chromatography-type septum sealing, and a protection trap (18a) equipped with a mechanical pump (18).

This vacuum system permits the extraction and trapping of plasma-generated active species and neutrals for analytical purposes. The sealing septum allows convenient sampling into a GC-MS instrument, and matching stainless steel tubing connections to the HR-MS feeding system allow introduction of a contamination-free sample. Needle valve (23) was used as a vent.

The plasma treatments were preceded by cleaning operations in the absence of substrates in order to remove possible contaminants from earlier experiments. The cleaning procedures involved heating up the lower electrode to 200°C and igniting the discharge in an oxygen environment (flow rate 15 sccm; pressure 250 mT; RF

power 200 W) for 10 minutes, followed by argon plasma discharge for 5 minutes (for complete removal of adsorbed oxygen), followed by cooling to room temperature. The upper electrode and the base plate of the reactor are provided with thermostating systems to limit extensive heating and to avoid damaging the electronic components located below the reactor. The plasma gases were introduced from reservoirs (1, 2, and 3) and the argon was supplied from container (4). Reservoir (5) was not used during the experiments. $SiCl_4$ was degassed by freezing it at liquid nitrogen temperature, vacuumed to base pressure level, and isolated by closing valve (6). During the experiments the containers were kept at room temperature. By correlating gas flowmeters (7 and 9) and valve (25), steady-state conditions were established between the incoming and outgoing flow rates.

In a typical experiment two paper surfaces were positioned symmetrically on the lower electrode, the upper part of the reactor was locked, and the reaction chamber was evacuated to base pressure level by operating the high capacity vacuum system. The second vacuum line was also operated but it was isolated from the reactor and outside environment by closing valves (21 and 23). Both traps were then cooled down to liquid nitrogen temperature and by operating valves (6), flowmeters (7 and 9), and the high cross-section valve (25). The pressure and flow rate from the selected plasma gas were established in the reactor at a steady-state rate. The plasma was then ignited, and the discharge was sustained for the desired time period. At the plasma ignition moment, valves (19 and 21) were opened and the gas sample collection was started. At the end of the trapping time, the trap and the whole second vacuum line were isolated from the plasma reactor by closing valves (19 and 21). At the end of the plasma treatment the RF power was disconnected, the flowmeter and gas feeding valves were closed, and the reactor was evacuated to base pressure level through open valve (25). The operation of both vacuum systems was then ceased, the vent valve was opened, and the paper samples and the collector trap (20) were removed from the system for analysis. The plasma-treated paper samples were stored under vacuum desiccator conditions until the characterizations were started. The experimental conditions employed during the plasma treatments were as follows:

Compounds selected for plasma treatments: CF_4, $SiCl_4$, and O_2
RF power dissipated to the electrodes: 60–175 W
RF frequency: 30 kHz
Base pressure: 40 mT
Pressure in the absence of plasma: 60–175 mT
Temperature of the substrate: 25°C
Flow rate of gases: 2.5–12 sccm
Trapping period: 2 minutes
Treatment time: 10 seconds–1 minute
Inert gas: argon

RESULTS AND DISCUSSIONS

Silicon Tetrachloride Plasma Treatment of Security Paper

Sized and unsized security paper were treated in a $SiCl_4$ plasma for various times, and the paper samples were characterized by ESCA, Wilhelmy wetting, and SEM. Typical comparative ESCA survey spectra of unsized and untreated SP, sized

and untreated SP, and $SiCl_4$-plasma-treated SP (pressure = 75 mT; power = 75 W; reaction time = 35 seconds) are shown in Fig. 2. The corresponding contact angle values and the surface atomic compositions are also presented in Fig. 2. The unsized and sized substrates show very similar ESCA spectra and surface atomic compositions (C1s = 58–59% and O1s = 36–38%). The slightly higher nitrogen content of the sized sample (5.4%) in comparison to the unsized substrate (2.6%) can be explained by the protein in the sizing material. It is noteworthy that the size results in a significant effect on the surface energy response. It diminishes the contact angle value by about 33%.

The ESCA and contact angle data for the $SiCl_4$-plasma-treated SP show significant differences in comparison to the nonirradiated substrates. The contact angle was reduced from 36.20° (Fig. 2a) to 11.18° (Fig. 2c) with the $SiCl_4$-plasma treatment. The $SiCl_4$-plasma treatment also modified the relative surface atomic composition; a much higher oxygen content (60.8%), a diminished carbon content (17.9%), and an intense silicon content (20.3%) can be noticed. A small chlorine peak was also detected which does not appear in Fig. 2(c). It is probable that Si—Cl groups are implanted at the surface and bury the carbon layer. These are likely converted to Si—OH functionalities on exposure to atmospheric moisture, as discussed below. The existence on the substrate surface of a small quantity of stable chlorine atoms can be explained through direct halogenation mechanisms from plasma-generated atomic chlorine.

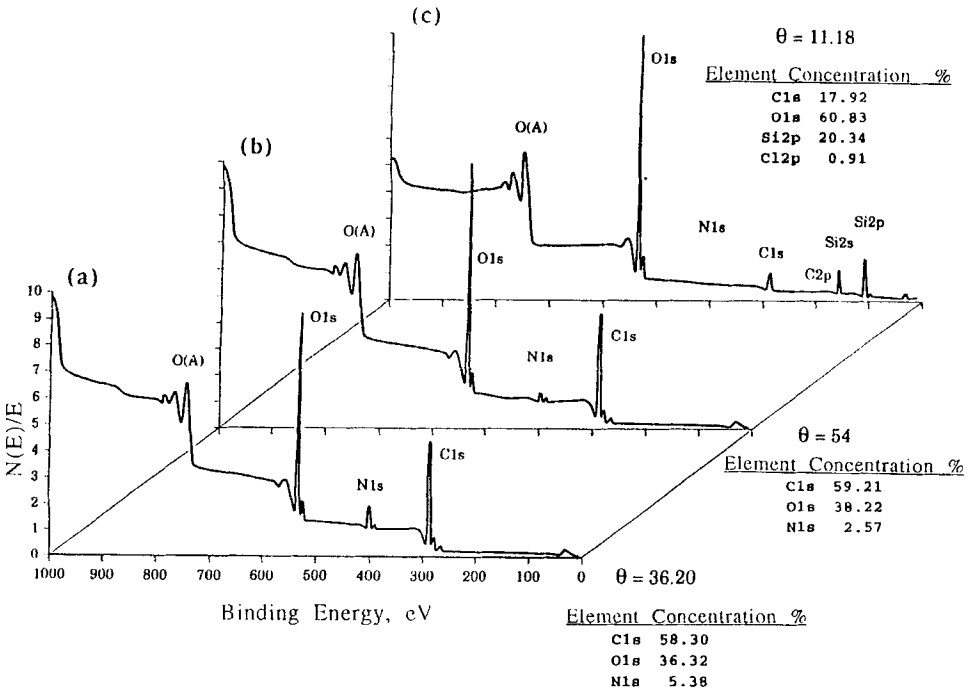

FIG. 2. ESCA comparative survey spectra of unsized and untreated SP (b), sized and untreated SP (a), and $SiCl_4$-plasma-treated SP (c), and the corresponding surface atomic composition and contact angle values.

Comparative high resolution ESCA C1s spectra of sized untreated SP (Fig. 3-1), of $SiCl_4$-plasma-treated sized SP at higher power and pressure levels (Fig. 3-2), and at lower power and pressure levels (Fig. 3-3) are shown in Fig. 3. The higher power and pressure treatment causes a significant diminution of the —C—OH peak (Fig. 3-2). Carbon hydroxyl functionalities were probably replaced by Si—Cl groups under the action of the plasma, and later converted into Si—OH functionalities under open laboratory conditions. The more significant presence of Si—OH groups on the paper surface (Si content = 20.3%) explains the low contact angle value (Fig. 3-3).

The central composite design in three blocks permitted the determination of the influence of interdependent modification factors on the contact angle values. However, because of experimental constraints, the actual experimental levels differ slightly from the original design. Five readings of contact angles were taken for each sample, and the median was used as the response to estimate the model. The average standard deviation of the contact angle determinations was 3.38 for treated samples. For control or untreated samples the same parameter was 2.51°. Table 1 shows the experimental factor levels, mean, median, and standard deviations of contact angles of silicon tetrachloride-plasma-treated samples.

The fitted empirical model is

$$\begin{aligned}\text{contact angle} = {} & 13.075\cdot\text{day}_1 + 12.62\cdot\text{day}_2 + 12.7\cdot\text{day}_3 - 1.73 \\ & \cdot\text{pressure} + 4.07\cdot\text{power} - 10.9\cdot\text{time} + 3.56\cdot\text{pressure}^2 \\ & + 7.86\cdot\text{power}^2 + 6.46\cdot\text{time}^2\end{aligned}$$

where day_i denotes indicator variables for the day when the experiment was run.

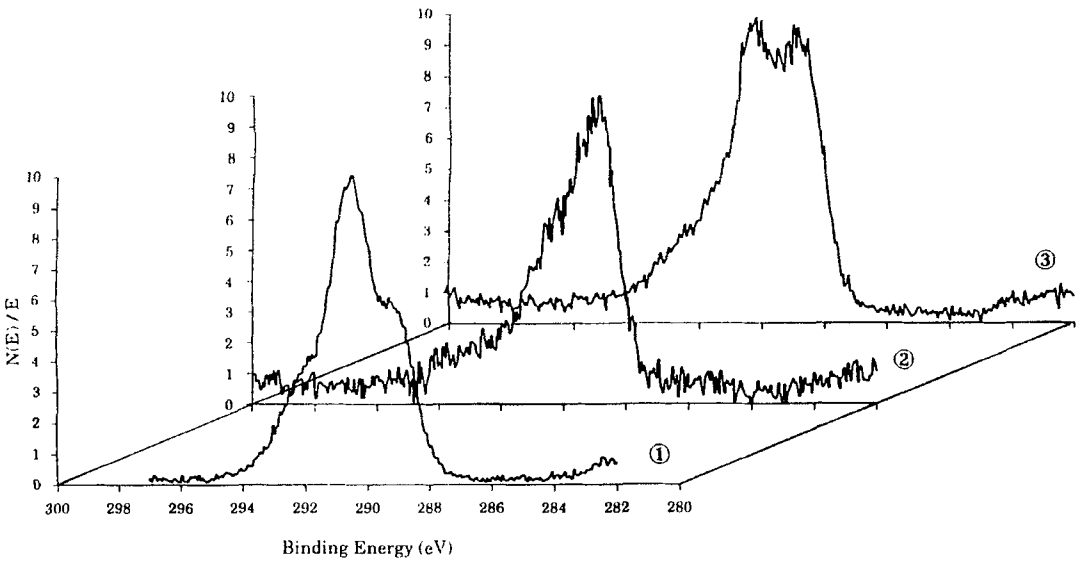

FIG. 3. Comparative high resolution ESCA C1s spectra of sized and untreated SP (1), and $SiCl_4$-plasma-treated sized SP at high power and pressure levels (2), and at low power and pressure levels (3).

TABLE 1. Experimental Factor Conditions, Contact Angles, and Atomic Concentrations for $SiCl_4$ Plasma Treatment

Experimental order	Day	Center	Pressure, mT	Power, W	Time, seconds	Contact angle			Atomic concentration					
						Mean	Median	Standard deviation	C	O	Si	N	C/O	C/Si
1	1	1	75	75	35	15.02	14.2	3.80	20.00	59.10	20.10	0.76	0.34	0.99
2	1	0	60	61	60	13.56	15.5	5.23	20.10	58.20	20.50	1.18	0.35	0.98
3	1	0	94	61	20	34.36	34.4	2.02	27.40	53.90	17.30	1.41	0.51	1.58
4	1	0	60	94	20	39.20	39.5	3.38	32.90	49.20	15.20	2.73	0.67	2.16
5	1	1	75	75	35	12.66	12.1	2.00	19.00	60.20	20.50	0.38	0.32	0.92
6	1	0	94	94	60	28.72	28.1	2.80	24.00	55.10	17.50	3.42	0.44	1.37
7	2	0	60	61	20	32.08	32.4	4.64	28.80	53.50	16.20	1.63	0.54	1.78
8	2	1	75	75	35	10.18	11.4	2.57	19.30	59.70	20.20	0.83	0.32	0.95
9	2	0	60	94	60	30.54	30.4	3.58	24.80	54.60	18.50	2.08	0.45	1.34
10	2	0	94	61	60	12.90	13.3	4.45	18.30	59.40	21.30	1.11	0.31	0.86
11	2	0	94	94	20	47.88	47.5	3.48	30.10	51.80	15.60	2.44	0.58	1.92
12	2	1	75	75	35	12.16	13.3	4.08	19.40	58.70	20.30	1.56	0.33	0.95
13	3	0	75	43	35	30.96	32.2	3.69	28.90	52.40	16.90	1.77	0.55	1.71
14	3	0	75	75	74	15.96	15.1	3.94	15.20	61.60	22.50	0.76	0.25	0.68
15	3	1	75	75	35	11.18	9.6	4.55	18.50	60.40	20.10	0.99	0.31	0.92
16	3	0	75	75	7	36.08	37.3	3.27	30.60	52.00	15.80	1.64	0.59	1.94
17	3	0	107	75	35	16.46	17.4	3.78	14.40	62.30	22.10	1.18	0.23	0.65
18	3	0	53	75	35	24.34	24.3	0.54	24.90	56.10	17.00	2.04	0.44	1.47
19	3	0	75	107	35	26.34	25.7	3.22	26.10	54.40	18.80	0.72	0.48	1.39
20	3	1	75	75	35	14.16	13.4	3.31	19.30	58.70	21.10	0.93	0.33	0.92
Control						35.50	36.2	2.15	59.50	36.00	0.00	4.44	1.65	
Control						33.94	34.6	2.67	58.00	35.40	0.00	6.56	1.64	
Control						39.08	40.8	2.70	58.60	36.60	0.00	4.81	1.60	
Control						37.86	38.1	1.78	58.40	36.30	0.00	5.34	1.61	

The variables pressure, power, and time have been centered and standardized such that the experimental region defined by the full factorial has 2 unit width in each parameter direction. The residual standard deviation is $s = 3.49$ and the multiple correlation coefficient $R^2 = 0.949$. All the estimated coefficients have observed significance less than 5% (p-value, the probability of the coefficient to be negligible). Assuming the reactor conditions are similar to the third day of experimentation, the minimum contact angle is 7.27 ± 0.52 (95% confidence interval) under the experimental conditions: pressure = 79.13 mT, power = 70.727 W, and time = 51.88 seconds. Figures 4–6 show the response surfaces and contour plots for the estimated contact angles. Because the factor levels were centered and standardized, the coefficients for quadratic terms are directly interpreted as a measure of the

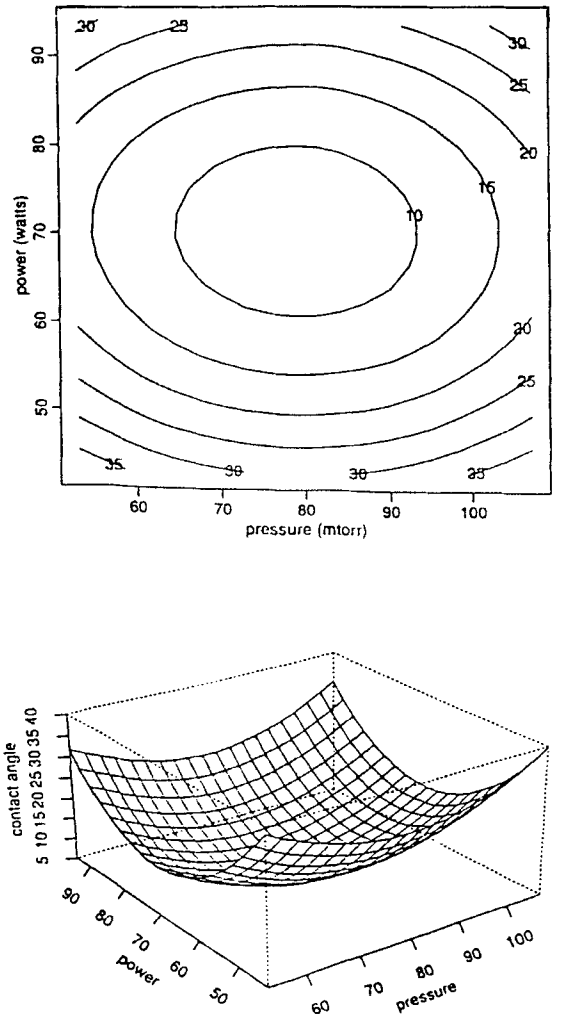

FIG. 4. Contour plot and response surface of contact angle for $SiCl_4$-plasma-treated SP (factor time is fixed at 52 seconds).

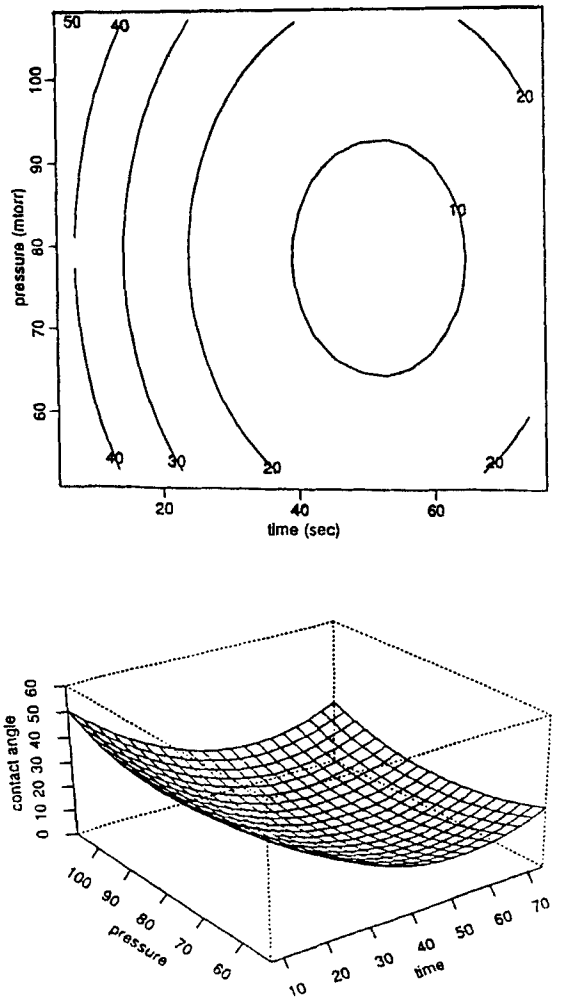

FIG. 5. Contour plot and response surface of contact angle for $SiCl_4$-plasma-treated SP (factor power is fixed at 72 W).

curvature of the contact angle response in each direction. The difference between the coefficients of pressure and time is apparent in Fig. 5.

In order to understand the relationship between the contact angle values and plasma-generated novel surface atomic compositions (created under different experimental conditions), contour plots and surface responses were also calculated for C/O and C/Si atomic ratios. Table 1 exhibits the atomic concentrations and the corresponding experimental conditions.

Because the atomic concentrations are expressed as percentages, whenever an element increases, the other ones should decrease. This constraint is reflected when linear correlations are computed. Therefore, we can expect similar behavior of some of the elements but in opposite directions. To break this dependence, we only

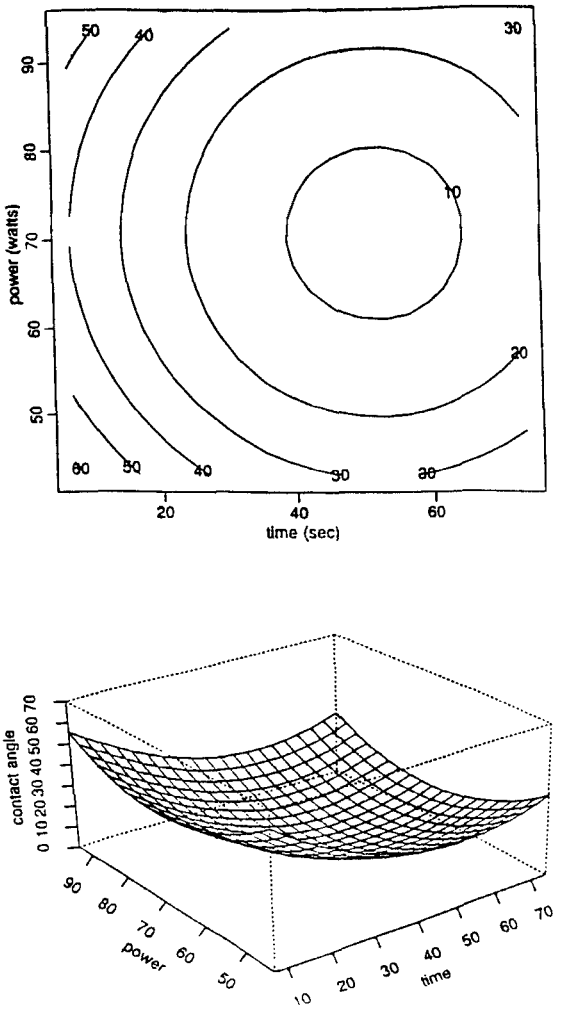

FIG. 6. Contour plot and response surface of contact angle for $SiCl_4$-plasma-treated SP (factor pressure is fixed at 79 mT).

consider the relationships between contact angle and the ratios C/Si and C/O. Table 2 shows the linear correlation of the contact angle with atomic concentrations of the elements and the ratios C/O and C/Si. One can notice a high correlation between contact angle and almost all the elements. High concentrations of Si and O on sample surfaces are associated with low contact angles and low carbon content. This fact can be seen in Fig. 7 which displays the scatter plots of contact angle, Si, and the ratios C/Si and C/O. In particular notice that Runs 14 and 17 are slightly away from general linear pattern. These samples correspond to the highest levels of time and pressure factors, indicating possible different mechanisms when operating under extreme pressure and treatment time conditions. As expected, a high correlation exists between Si atom concentrations and C/O atomic ratios ($r = 0.946$).

TABLE 2. Linear Correlation between Contact Angle and Atomic Concentrations

C	O	Si	N	C/O	C/Si
0.906	−0.917	−0.893	0.688	0.917	0.922

A second-degree polynomial was used to model the C/O ratio based on the process pressure, power, and treatment time. Similar to the contact angle behavior, no interaction effects were apparent. The fitted model is

$$C/O = 2.80 \cdot day_1 + 2.78 \cdot day_2 + 2.80 \cdot day_3 - 0.017 \cdot pressure - 0.0359 \cdot power - 0.0174 \cdot time + 0.0001 \cdot pressure^2 + 0.0002 \cdot power^2 + 0.0002 \cdot time^2$$

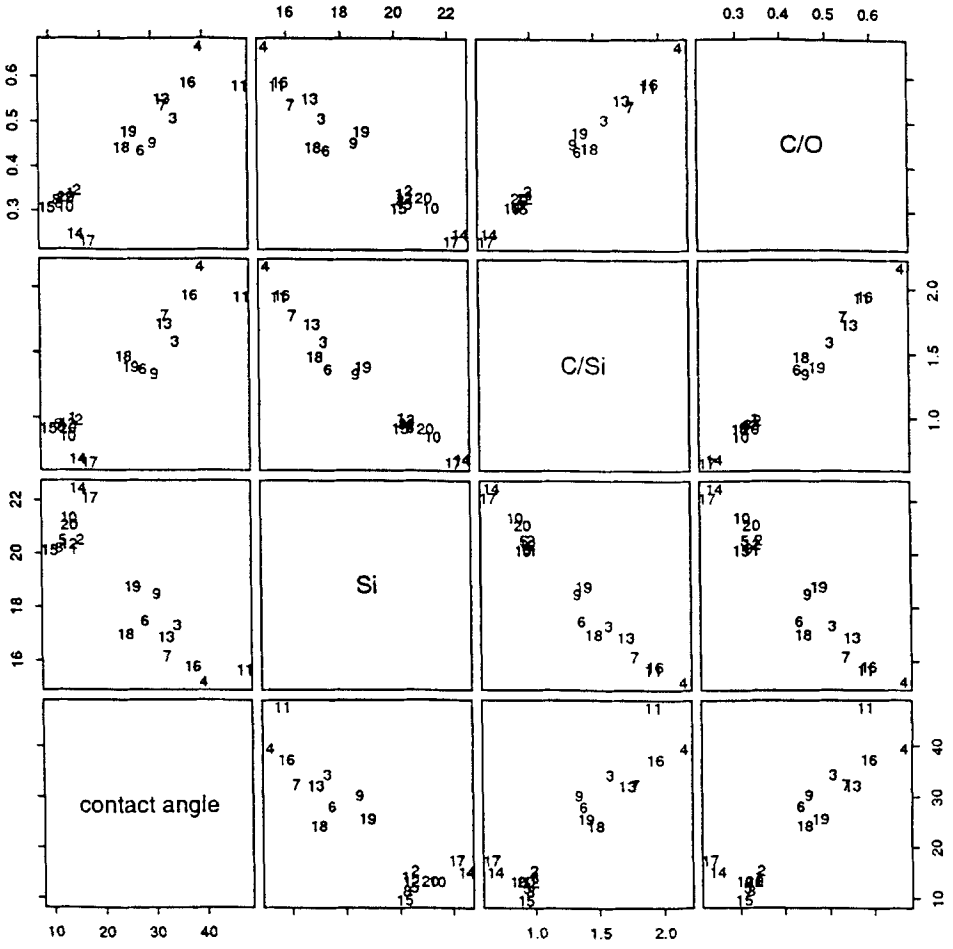

FIG. 7. Scatter plots for contact angle and atomic composition for Si, and the ratios C/Si and C/O. The labels indicate the sample numbers.

where the factors are considered in original scales. The residual standard deviation is $s = 0.0499$ and $R^2 = 0.91$. The estimated coefficients have p-values less than 1%, with the exception of pressure^2 at 9%. As it can be seen in Fig. 7, Samples 14 and 17 have the lowest values of C/O (highest oxygen concentration), and this result is slightly different from the general trend. These samples correspond to the highest levels of time and pressure, respectively. Figures 8–10 exhibit the contour plots and response surfaces of the fitted C/O ratios about the center of the design.

The C/Si ratios are similarly positively correlated to the contact angle, and similar model fits were expected. Samples 14 and 17 show the highest Si concentration. The fitted quadratic model is

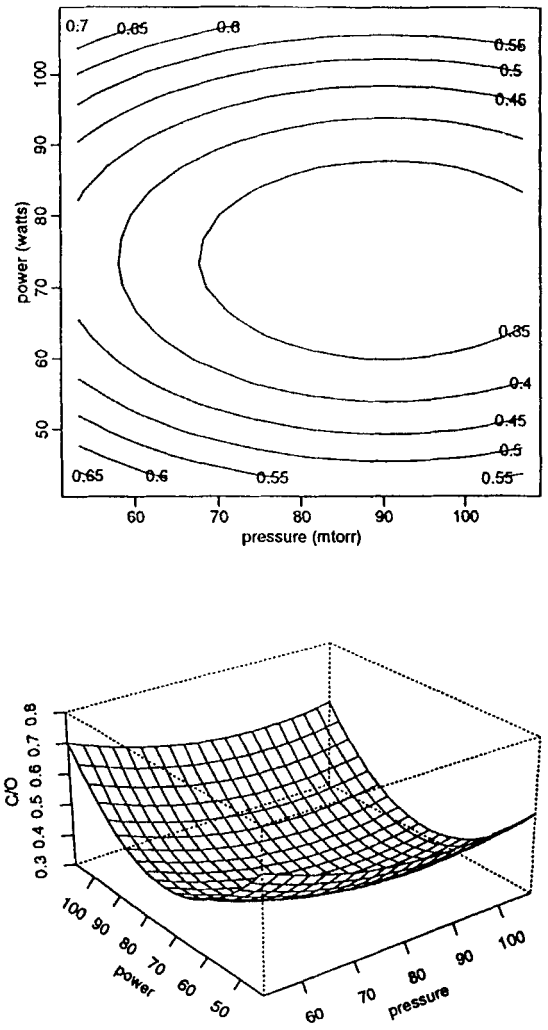

FIG. 8. Contour plot and response surface of C/O for $SiCl_4$-plasma-treated SP (factor time is fixed at 35 seconds).

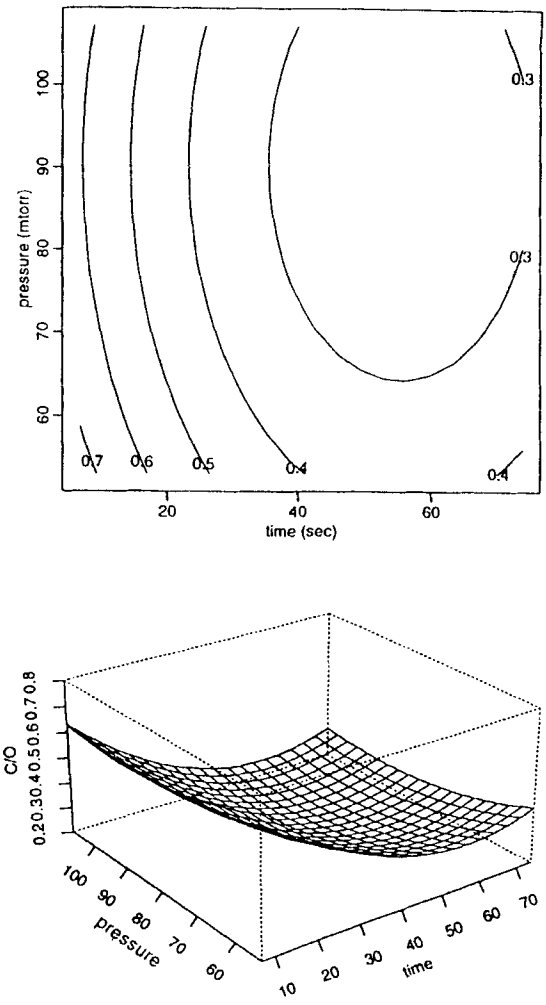

FIG. 9. Contour plot and response surface of C/O for $SiCl_4$-plasma-treated SP (factor power is fixed at 75 W).

$$\begin{aligned} C/Si = {} & 10.22 \cdot day_1 + 10.18 \cdot day_2 + 10.23 \cdot day_3 - 0.051 \cdot pressure - \\ & 0.155 \cdot power - 0.059 \cdot time + 0.0003 \cdot pressure^2 + 0.0011 \cdot power^2 \\ & + 0.005 \cdot time^2 \end{aligned}$$

where the factors are expressed in original scales. The residual standard deviation is $s = 0.138$ and $R^2 = 0.95$. Estimated coefficients have p-values less than 1%, with the exception of pressure^2 which is 8%. The fitted contour plots and response surfaces are exhibited in Figs. 11–13.

The atomic concentrations show similar behavior to the contact angle but in the opposite direction, as seen in Fig. 7. For example, if silicon or oxygen contents are high (and therefore carbon content is low), the ratios C/Si or C/O are low

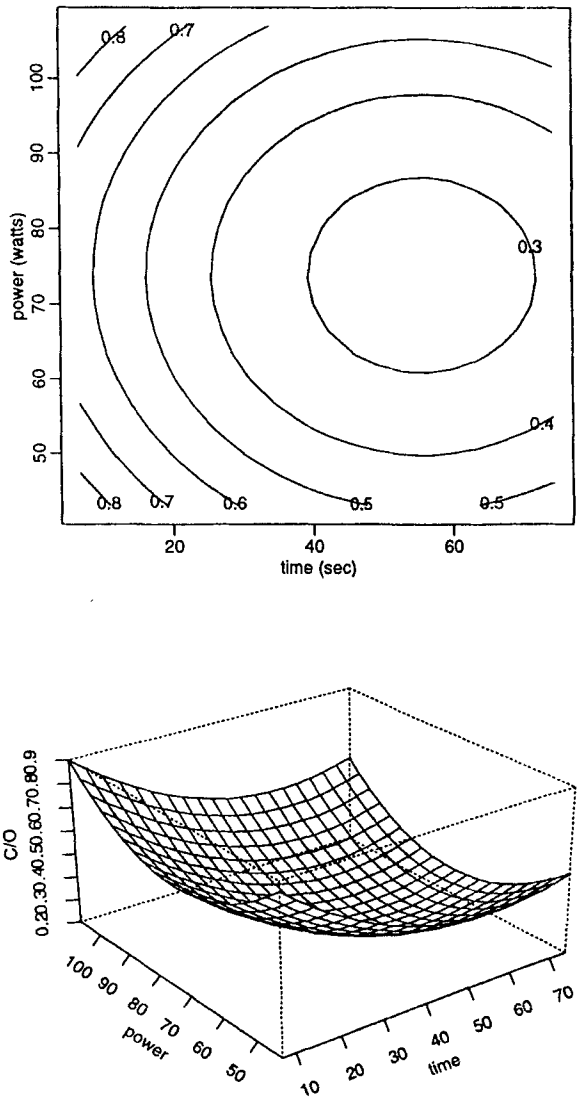

FIG. 10. Contour plot and response surface of C/O for $SiCl_4$-plasma-treated SP (factor pressure is fixed at 75 mT).

respectively and so is the contact angle. Of course, all factors and/or mechanisms are not captured in this empirical model.

Mechanisms of $SiCl_4$ Plasma Modification

For determination of mechanisms of silicon tetrachloride plasma reactions, the formation of the ionic fragments was simulated by MS-electron-induced fragmentation. The MS-electron and plasma-induced fragmentation mechanisms are

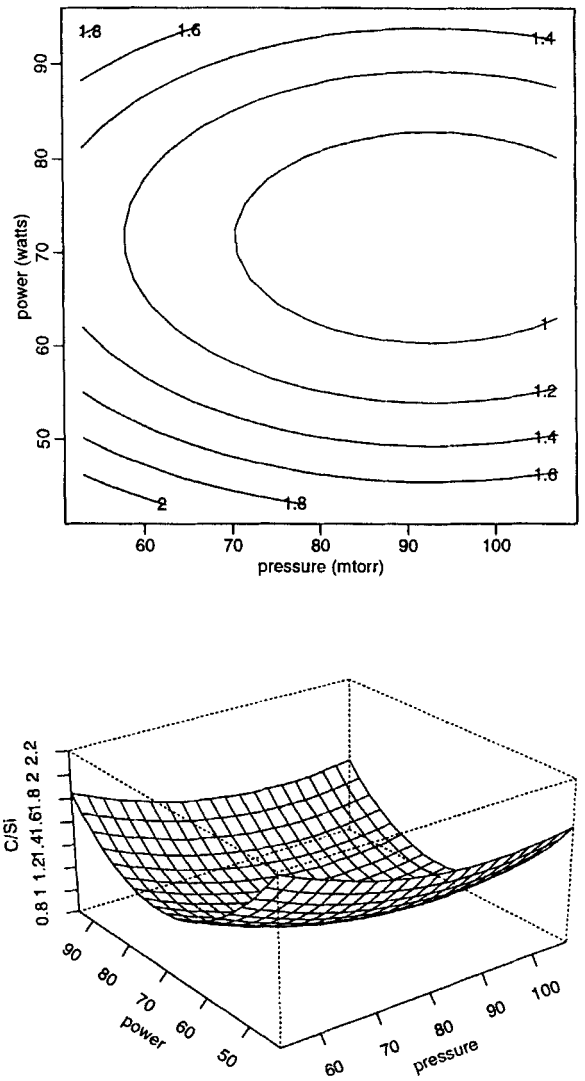

FIG. 11. Contour plot and response surface of C/Si for $SiCl_4$-plasma-treated SP (factor time is fixed at 35 seconds).

not identical; however, our experimental data indicate striking similarities [27-31]. If one assumes that the electron energy distribution in the plasma and the ion source energy of the mass spectometer are comparable, then the relative ratios of plasma-generated species can be predicted.

Figure 14 exhibits a typical LEEMS fragmentation pattern of $SiCl_4$ and the corresponding electron-energy-dependent ionic-fragment composition. It can clearly be noticed that the most predominant ionic fragment is $m/e = 135$ [$-Si(Cl)_3^+$] and that the concentration of lower m/e fragments (98 and 63) are negligible. The

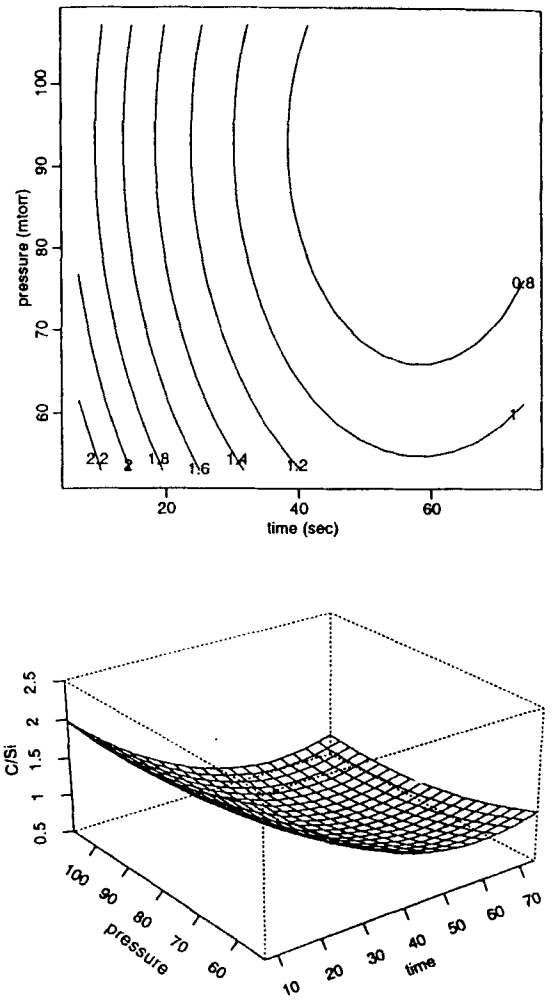

FIG. 12. Contour plot and response surface of C/Si for $SiCl_4$-plasma-treated SP (factor power is fixed at 75 W).

presence of molecular ion (m/e = 170) can also be noticed; where the relative ratio of this fragment is greater at low electron-energies (30 eV). $Si(Cl)_x$-based cations are extremely reactive; they can react even with the most inert substrate surfaces such as polypropylene. At the same time, the Si—Cl bonds are very unstable under open laboratory conditions. In the presence of water molecules (e.g., moisture) they are readily transformed into Si—OH functionalities. This behavior is significant because it opens up new possibilities for functionalizing a large variety of substrates. Hydrophilicity and improved adhesion characteristics can be achieved by increasing the polar components of the surface energy. Si—Cl linkages also permit the development of second-stage grafting reactions with organosilicon monomers.

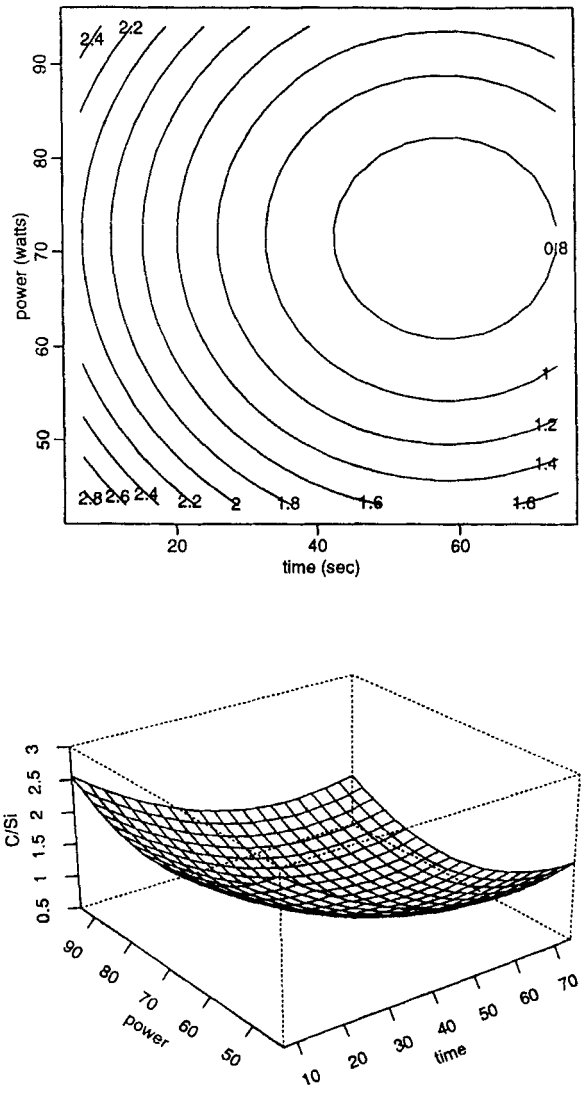

FIG. 13. Contour plot and response surface of C/Si for $SiCl_4$-plasma-treated SP (factor pressure is fixed at 75 mT).

Oxygen Plasma Treatment of Security Paper

A typical ESCA survey spectrum of oxygen-plasma-treated security paper is shown in Fig. 15 (pressure = 175 mT, power = 61 W, and treatment time = 20 seconds). The surface atomic composition of the modified sample and the corresponding contact angle value (θ = 10.32) are also presented in Fig. 15. Plasma-generated active oxygen atoms are extremely reactive and consequently the presence of a high oxygen content at the surface (51.9%) was expected. This value represents an approximately 40% oxygen content increase at the surface of the paper in com-

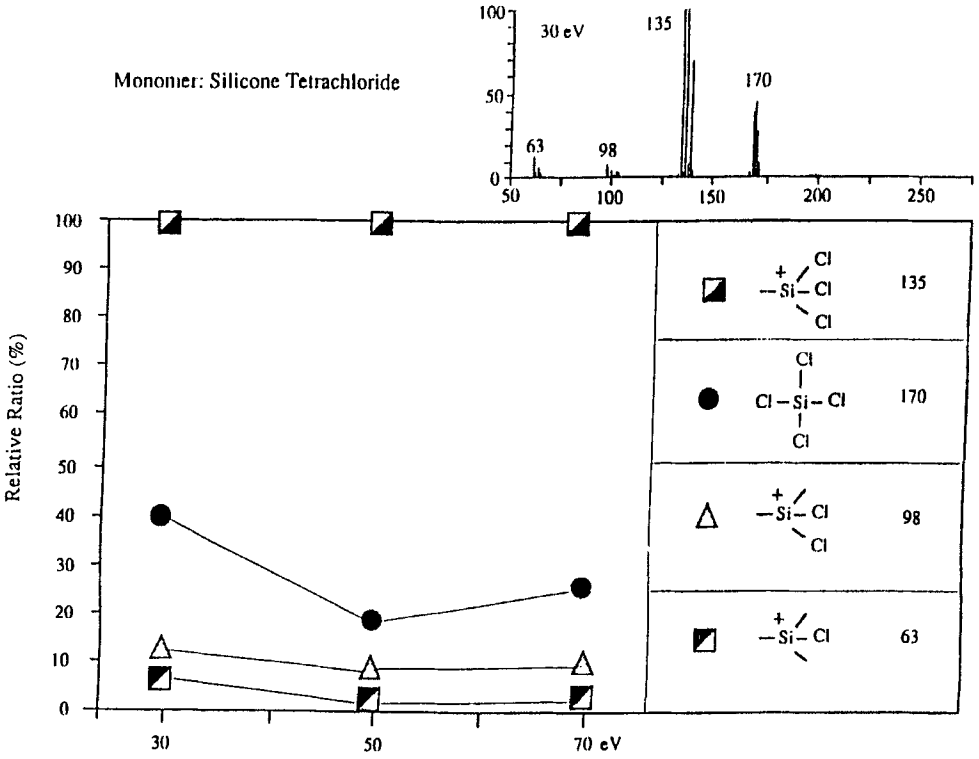

FIG. 14. LEEMS fragmentation pattern of $SiCl_4$ and the corresponding electron-energy-dependent ionic-fragment composition.

parison to the untreated substrates. As a consequence, the carbon content is diminished to 43.8%. It is interesting to note that the active oxygen species do not influence significantly the nitrogen content of the sized currency paper samples (4.23%), while $SiCl_4$-plasma completely removed this atomic species.

A high resolution ESCA C1s spectra of oxygen-plasma-treated sized SP (at high pressure and low power levels) is shown in Fig. 16-1; the spectrum at lower pressure and high power is shown in Fig. 16-2. The lowest contact angle was obtained at high pressure and low power. The results in Fig. 16 indicate that possible —C—O—C— linkage scission reactions associated with ring opening and subsequent —C=O formation mechanisms (Fig. 16-2) may be responsible for the rearrangement of the surface atomic composition. Previous work has also shown that plasma-generated surface —C=O functionalities lead to better adhesion characteristics [32], in good agreement with the existence of low contact angle values.

A blocked central composite design was also selected to assess the influence of the process factors on the wettability characteristics of the security paper. The first half of the 2^3 factorial design was repeated for confirmation (Days 1 and 2). Table 3 exhibits the experimental conditions and corresponding contact angles. The average standard deviation of the contact angles per treated surface was 3.76.

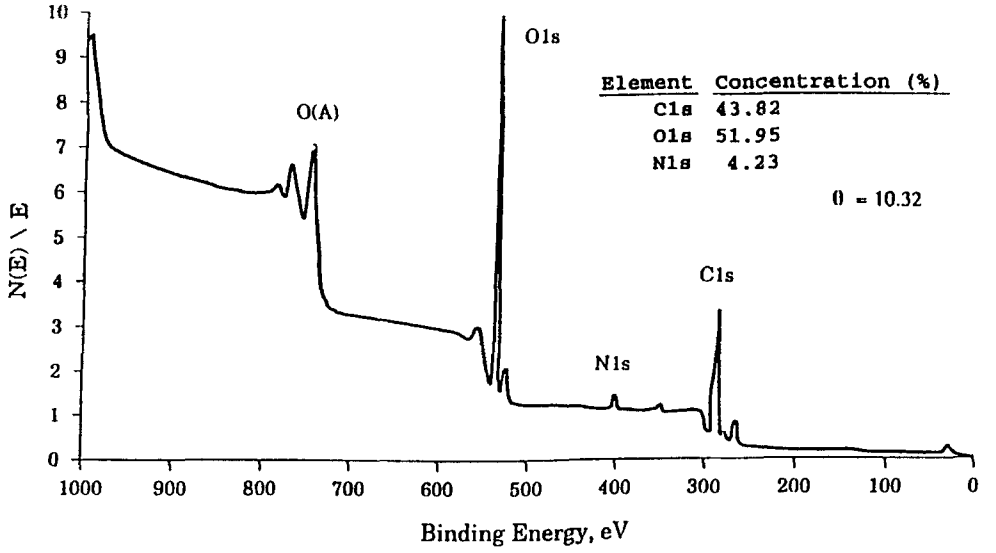

FIG. 15. Typical ESCA survey spectrum of oxygen-plasma-treated SP, and the surface atomic composition and corresponding contact angle values.

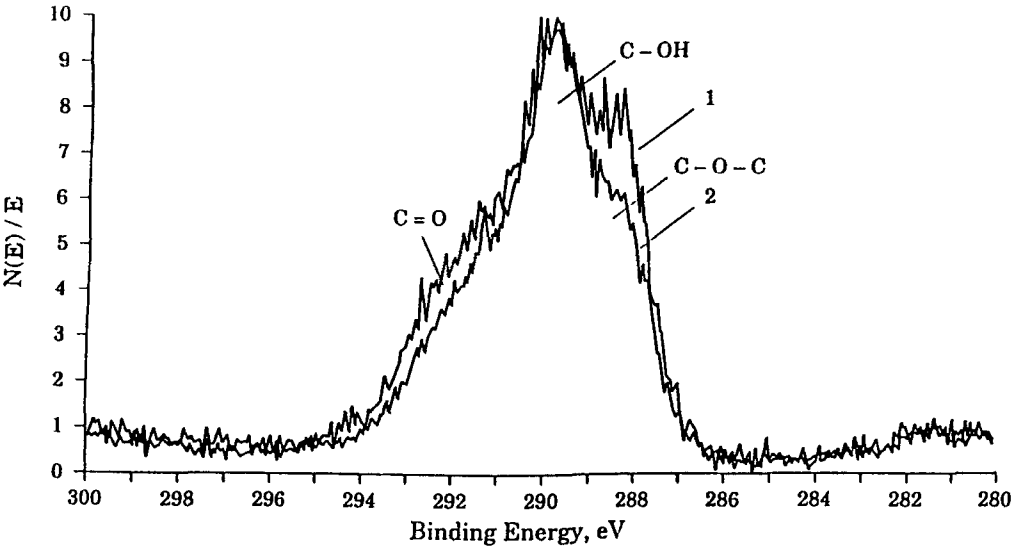

FIG. 16. High resolution ESCA C1s spectra of oxygen-plasma-treated sized-SP at high pressure and low power levels (1), and at low pressure and high power levels (2).

TABLE 3. Experimental Conditions and Contact Angles for O_2 Plasma Treatment

Experimental order	Day	Center	Pressure, mT	Power, W	Time, seconds	Contact angle		
						Mean	Median	Standard deviation
1	1	1	145	75	35	14.0	15.5	3.27
2	1	0	115	61	50	15.4	14.4	5.16
3	1	0	175	61	20	13.4	13.5	2.80
4	1	0	115	89	20	38.5	39.1	5.15
5	1	1	145	75	35	18.5	18.9	5.54
6	1	0	175	89	50	12.8	11.7	4.45
7	2	0	175	89	50	12.2	13.9	5.55
8	2	0	115	89	20	55.0	56.3	6.89
9	2	1	145	75	35	28.0	27.9	3.66
10	2	0	175	61	20	10.3	8.1	4.65
11	2	1	145	75	35	26.5	25.9	3.74
12	3	0	115	61	20	29.1	29.1	3.10
13	3	1	145	75	35	15.6	17.5	3.70
14	3	0	115	89	50	29.1	29.7	2.09
15	3	0	175	61	50	15.5	16.5	3.00
16	3	0	175	89	20	16.8	16.0	4.41
17	3	1	145	75	35	17.7	17.6	2.78
18	3	0	115	61	50	17.9	18.8	3.39
19	4	0	195	75	35	8.3	10.4	4.69
20	4	1	145	75	35	26.1	26.8	3.19
21	4	0	145	51	35	24.2	24.5	2.79
22	4	0	94	75	35	56.2	56.6	2.44
23	4	0	145	75	60	30.8	30.0	3.22
24	4	0	145	98	35	46.8	47.6	1.99
25	4	0	145	75	10	35.1	37.3	3.35
26	4	1	145	75	35	24.7	24.6	2.87

The analysis of oxygen-plasma treatments showed that control factors interact in multiples on the contact angles. This fact is reflected by the interaction terms. The estimated model is

$$\begin{aligned}\text{contact angle} = {} & 5.68\cdot\text{day}_1 + 2.019\cdot\text{day}_2 + 4.89\cdot\text{day}_3 + 2.31\cdot\text{day}_4 \\ & + 0.0174\cdot\text{pressure} + 1.61\cdot\text{power} - 1.32\cdot\text{time} \\ & - 0.00865\cdot\text{pressure:power} + 0.00781\cdot\text{pressure:time}\end{aligned}$$

with an estimated standard deviation of $s = 5.29$, and $R^2 = 0.89$. Under reactor performance similar to Day_4, the minimum estimated contact angle within the factorial part of the experimental conditions was 11.92 ± 3.44 (95% confidence interval), for pressure = 175 mT, power = 61 W, and time = 20 seconds. Keeping pressure and power levels fixed and changing time to 50 seconds, the estimated contact angle was $13.12 \pm 5.39°$. Thus, the contact angle is not very sensitive to

variations in treatment time for oxygen-plasma treatment of the paper. Figures 17–19 show the response surfaces and contour plots for the contact angle about these later experimental conditions.

Carbon Tetrafluoride Plasma Treatment of Security Paper

All the CF_4-plasma-treated security paper exhibited a high surface fluorine content. A typical ESCA survey spectrum of a carbon tetrafluoride-plasma-modified sample is shown in Fig. 20 (pressure = 175 mT, power = 89 W, treatment time = 50 seconds). The corresponding surface atomic composition and contact angle value (θ = 120.56°) are also presented in Fig. 20. The significant

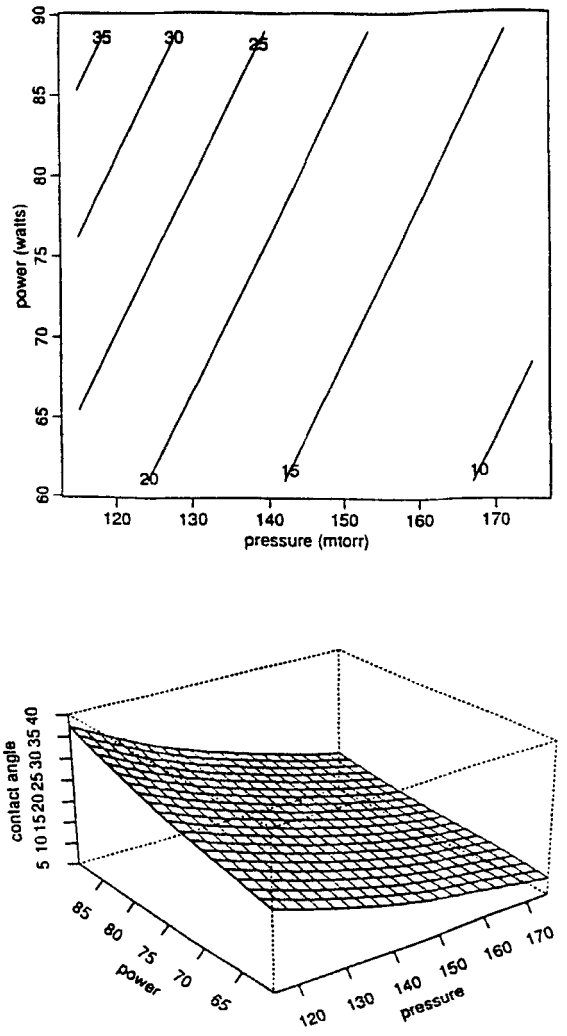

FIG. 17. Contour plot and response surface of contact angle for oxygen-plasma-treated SP (factor time is fixed at 50 seconds).

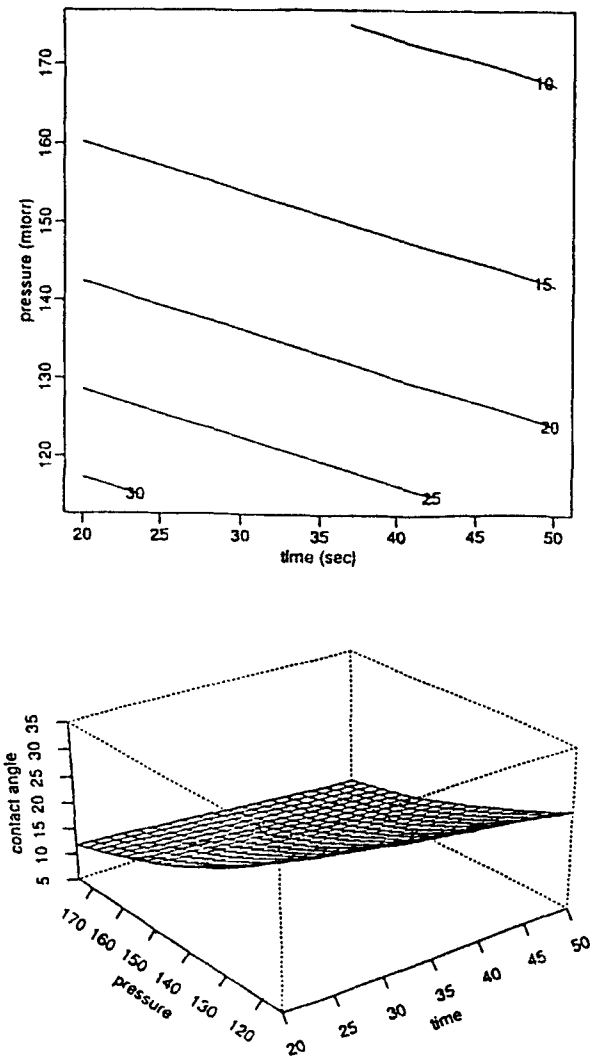

FIG. 18. Contour plot and response surface of contact angle for oxygen-plasma-treated SP (factor power is fixed at 61 W).

decrease of carbon (45.9%) and oxygen (19.9%) concentration of the plasma-irradiated substrate in comparison to the sized control-sample (59.2% carbon and 36.2% oxygen), and the presence of a high fluorine content (30.6%), obviously indicate the development of an intense plasma-induced surface fluorination mechanism. Fluorinated surfaces usually exhibit a strong hydrophobic character, which is also reflected in high contact angle values. The very high contact angle (θ = 120.56°) of the CF_4-plasma-treated sample again demonstrates the presence of a hydrophobic surface. Due to the intense fluorine-mediated ablation reactions developed under RF-plasma conditions, surface fluorination reactions (high fluorine content) do not always reflect diminished adhesive characteristics [33]. Unsaturated

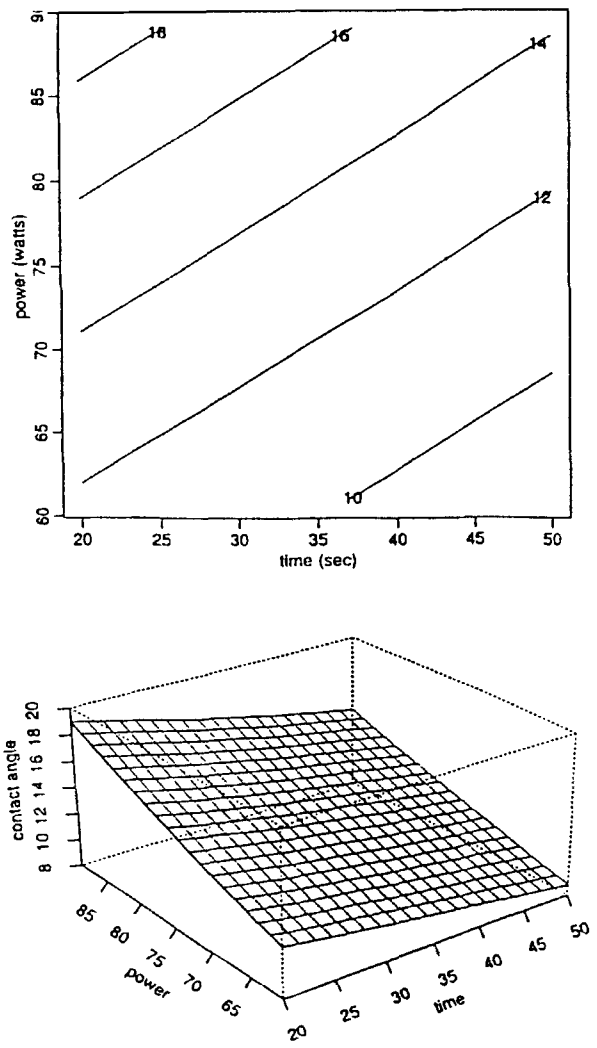

FIG. 19. Contour plot and response surface of contact angle for oxygen-plasma-treated SP (factor pressure is fixed at 175 mT).

bonds and trapped free radicals (associated with an intensified surface roughness) generated by dehydrogenation and chemical bond-scission reactions can also lead to improved adhesion behavior through postplasma oxidation mechanisms (e.g., improved dyeing or printing properties).

The high resolution C1s ESCA spectrum of CF_4-plasma-treated samples (Fig. 21) clearly shows the development of intense fluorination. The broad peak between 293 and 300 eV binding energy values, associated with the main C1s peak, indicates the presence of CF_x functionalities.

A 2^3 factorial design in two blocks (day) and center points was used for investigating the influence of CF_4-discharge parameters. The experimental condi-

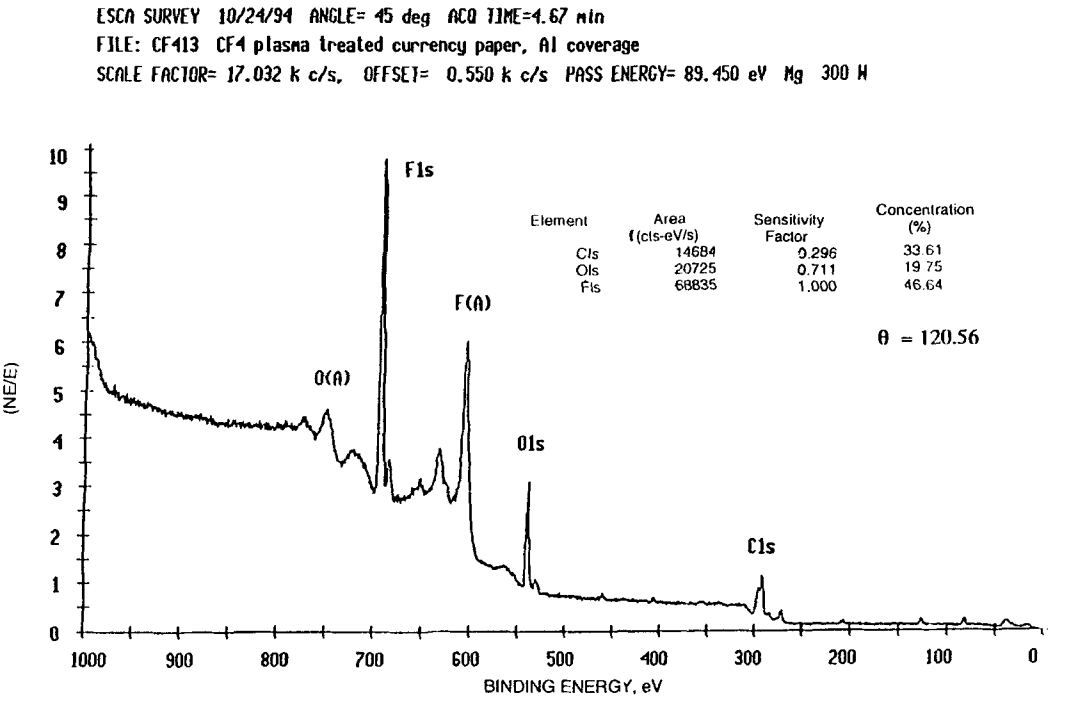

FIG. 20. Typical ESCA survey spectrum of CF_4-plasma-treated SP, and the corresponding surface atomic composition and contact angle values.

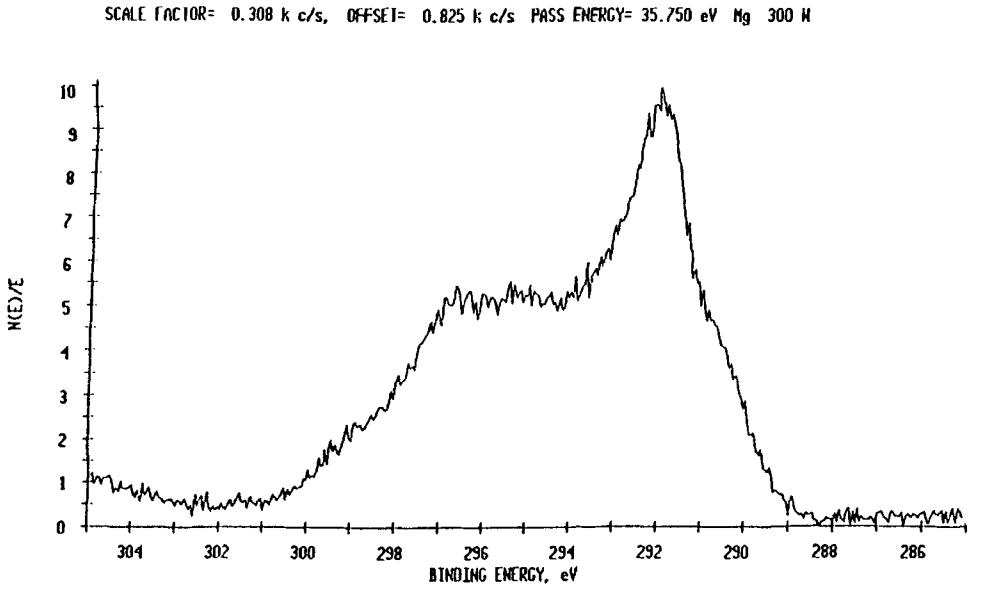

FIG. 21. High resolution C1s ESCA spectrum of CF_4-plasma-treated SP.

tions and contact angles are exhibited in Table 4. The average standard deviation of the measures of contact angle per sample is 5.26. The observed contact angle values are much higher in comparison to the untreated sample. These results are not surprising since even the slightest fluorination will induce an intense hydrophobic character. However, an empirical model was fitted to assess the influence of the process parameters on contact angle. Interaction between pressure and power was found significant. The fitted model is

$$\text{contact angle} = 109.6 - 0.6\cdot\text{day} - 4.3\cdot\text{center} + 2.23\cdot\text{pressure} + 4.48\cdot\text{power} + 4.6\cdot\text{time} + 1.43\cdot\text{pressure:power}$$

with $s = 0.51$ and $R^2 = 0.99$. Under similar conditions to the second day, the minimum estimated contact angle is $103.5 \pm 2.6°$ (95% confidence interval), at pressure = 115 mT, power = 61 W, and time = 20 seconds. Figures 22–24 present the response surfaces and contour plots for estimated contact angles at the center of the experimental region.

Surface Energy Components of Plasma-Treated Security Paper

Besides the specific surface area, the chemical nature of a surface, manifested by surface energy components, controls the wetting and adhesion. The balance of dispersion (van der Waals interactions) and polar forces (dipole-dipole interactions, hydrogen bonding, acid-base interactions, etc.) from surface functionalities establish the surface free energy levels. By estimating the relative ratios of these components, significant surface interactions can be interpreted and predicted. The respective polar and dispersive surface free energies can be evaluated by measuring the fiber wetting force in two different probe liquids such as water and methylene iodide and solving the simultaneous equations proposed by Wu [34] according to a reciprocal means approach.

TABLE 4. Experimental Conditions and Contact Angles for CF_4 Plasma Treatment

Experimental order	Block day	Block center	Pressure, mT	Power, W	Time, seconds	Contact angle		
						Mean	Median	Standard deviation
1	1	0	175	61	20	100.34	100.41	0.36
2	1	0	175	89	50	120.56	121.11	1.52
3	1	1	145	75	35	104.92	105.21	1.99
4	1	0	115	89	20	105.18	105.21	2.38
5	1	1	145	75	35	104.88	105.01	1.38
6	1	0	115	61	50	108.62	108.61	0.88
7	2	1	145	75	35	103.64	104.41	1.35
8	2	0	175	61	50	110.54	109.71	3.20
9	2	0	115	61	20	97.08	98.31	3.42
10	2	1	145	75	35	103.96	103.01	2.61
11	2	0	115	89	50	115.34	113.91	2.56
12	2	0	175	89	20	112.86	112.61	2.71

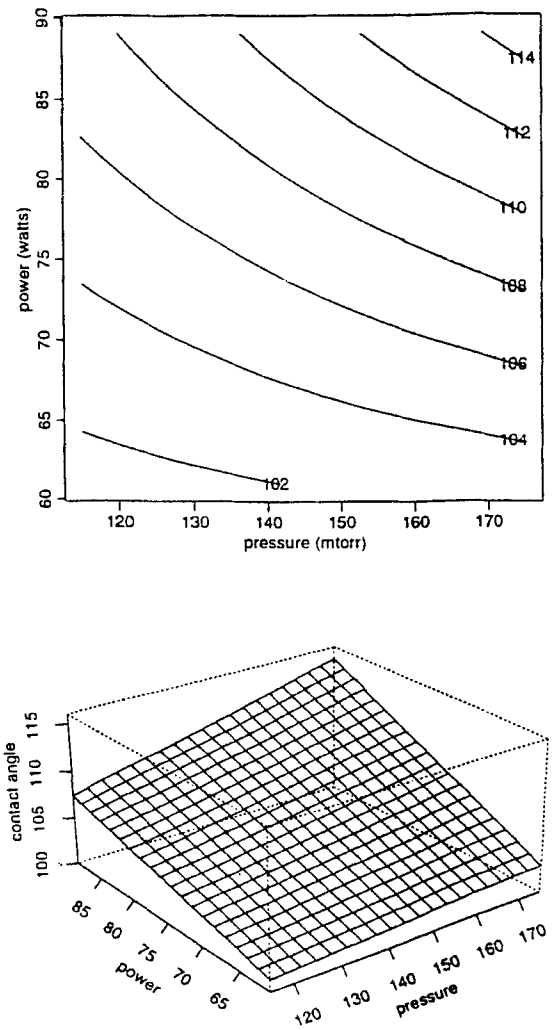

FIG. 22. Contour plot and response surface of contact angle for CF_4-plasma-treated SP (factor time is fixed at 35 seconds).

Recently it has been shown that the polar components can be separated into Lewis acid and base terms [8]. The calculation of the acid/base components of wetting are given in Table 5. Complete wetting (ideal adhesion) occurs when $\theta = 0°$ or $(1 + \cos\theta) = 2$, while nonwetting occurs when $\theta > 90°$ or $(1 + \cos\theta) < 1$. Polar interactions can be either attractive or repulsive, consequently the $(1 + \cos\theta)$ value will be higher or lower depending on the relative magnitude of Lewis force components. Stronger adhesion results when two interfaces have an opposite acid-base character.

Table 5 summarizes the total and compositional surface energy values with the corresponding minimum contact angle data and experimental plasma-parameters for the untreated and plasma-treated SP samples. In comparison to the untreated

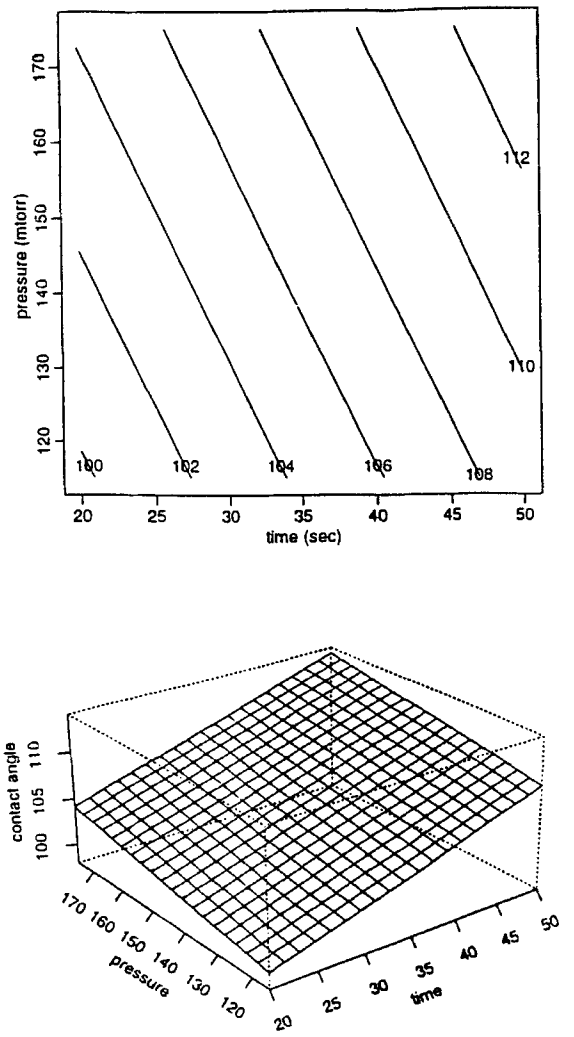

FIG. 23. Contour plot and response surface of contact angle for CF_4-plasma-treated SP (factor power is fixed at 75 W).

paper, one can notice a significant increase in the dispersion force participation for oxygen-treated paper and a dramatic decrease of this component for CF_4-plasma-modified paper. The $SiCl_4$-plasma-treated paper did not show a significant change in the dispersion force value. Acid and base polar force components also show different effects under different plasma conditions. Significant acid/base component increases were found with CF_4 and $SiCl_4$ plasmas, while O_2 plasma treatment gave reduced acid/base contributions. These results for oxygen plasma treatment (increased dispersion forces, reduced polar, and acid/base contributions) are contrary to what would be expected for the large reduction in contact angle and can be explained in two ways: that other factors are responsible for reduction of the contact

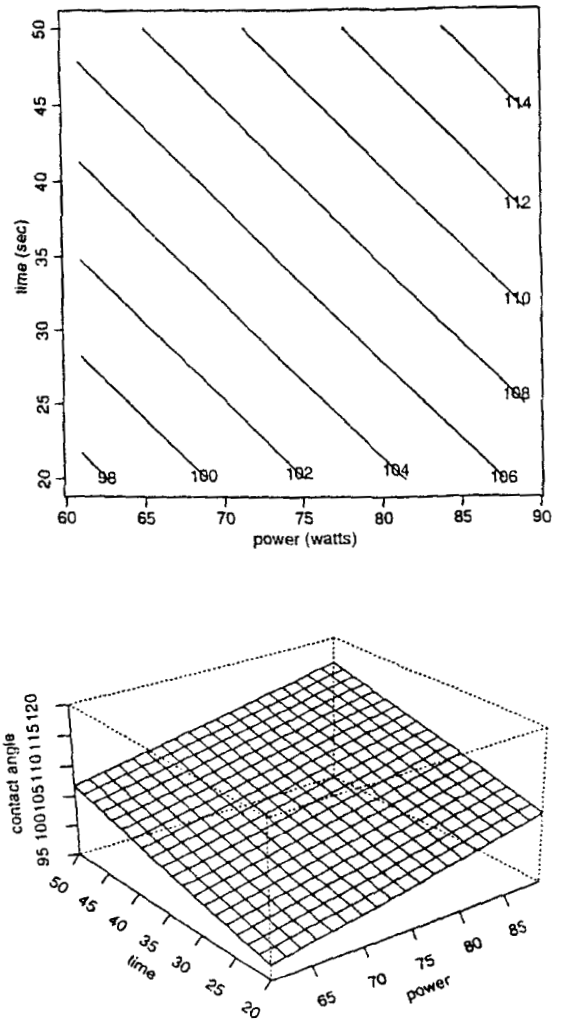

FIG. 24. Contour plot and response surface of contact angle for CF_4-plasma-treated SP (factor power is fixed at 145 mT).

angle or that the probe liquids (formamide, ethylene glycol, methylene iodide) are not suitable for characterization of these types of treatments. Future work is planned with additional probe liquids for the treated substrates.

Based on the contact angle data it is predicted that oxygen plasma-treated samples will have the most active surfaces; however, under certain experimental conditions, comparable adhesion characteristics may result from $SiCl_4$-plasma-treated samples. However, surface characterization may not totally predict bonding since many other factors related to the physical and chemical nature of the interfaces also affect adhesion characteristics.

TABLE 5. Comparisons of Work of Adhesion for Three Plasma-Treated Security Papers

	Treatment*				
	W^{d}, dyn/cm	W_a^{ab}, dyn/cm	W_b^{ab}, dyn/cm	W_a, dyn/cm	W_b, dyn/cm
Control	80.32	31.55	11.61	112.91	91.93
O_2 plasma†	97.22	16.56	−2.1	115.56	95.82
$SiCl_4$ plasma	77.97	36.87	17.06	115.30	95.03
CF_4 plasma	13.42	87.55	53.63	101.16	67.05

*The experimental conditions of plasma treatments for each gas are:
O_2 plasma: 61 W (power), 175 mT (pressure), and 20 seconds (time)
$SiCl_4$ plasma: 75 W (power), 75 mT (pressure), and 35 seconds (time)
CF_4 plasma: 89 W (power), 175 mT (pressure), and 50 seconds (time)
†The corresponding contact angles with water for each gas are:
O_2 plasma: 10.32°
$SiCl_4$ plasma: 12.66°
CF_4 plasma: 120.56°

Surface Morphology of Plasma-Treated Substrates

In addition to surface chemical modifications, energetic plasma particles (ions, electrons, excited species, etc.) induce ablation processes through bond-scission reactions. Low molecular weight, high volatility fragments formed by the action of the plasma species will constantly be removed from the plasma zone, leaving behind peculiar surface topographies. In the case of fibrous materials (natural and synthetic polymeric substrates), amorphous parts of the samples will be more intensely eroded and, as a result, more ordered crystalline zones will be exposed. The maximum area of contact between two surfaces or phases occurs when the adhesives penetrate the cavities or when liquid-phase components fill out crevices.

Scanning electron micrographs (produced at ×800 and ×10,000 magnification) of the untreated and treated SP substrates (Figs. 25–28) reveal changes in the surface morphology of $SiCl_4$-, O_2-, and CF_4-plasma modified substrates. Figures 26–28 exhibit somewhat rougher surfaces on the fibers in comparison to the sized-unmodified samples (Fig. 25). Lower magnifications reveal a more intense fibrous aspect, while higher magnifications show rougher surfaces on the fibers. A higher specific surface area, as well as surface chemical functionalization, can play a significant role in improved adhesion.

Print Screening of Plasma-Treated Security Paper

Oxygen and silicon tetrachloride-treated SP were evaluated in a print screening test. The treated paper samples were taped into areas of production sheets for printing with security ink. Two printed samples from each treatment were obtained, with one sample submitted for crumple rating after 16 crumples and the other sample submitted for sodium hydroxide solution soak tests. As shown in Table 6,

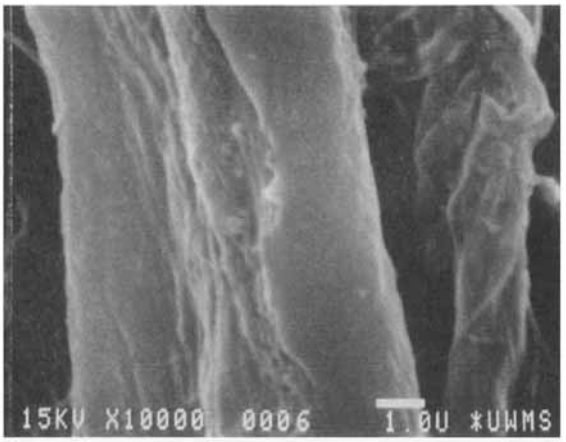

A

B

FIG. 25. Scanning electron micrographs of untreated and sized SP samples at ×800 (a) and ×10,000 (b) magnifications.

the oxygen plasma-treated sample provided superior results to the silicon tetrachloride-treated paper. Crumple ratings of 6 (top of rating scale) were achieved, and the sodium hydroxide soak results were superior to the standard for oxygen plasma treatment #1. The crumple ratings for the silicon tetrachloride-treated paper were lower than the treated control.

CONCLUSIONS

RF-cold plasma conditions are suitable for surface modification of sized and unsized security paper substrates. Oxygen-plasma treatments resulted in a significant decrease in contact angle values under all experimental conditions. Higher

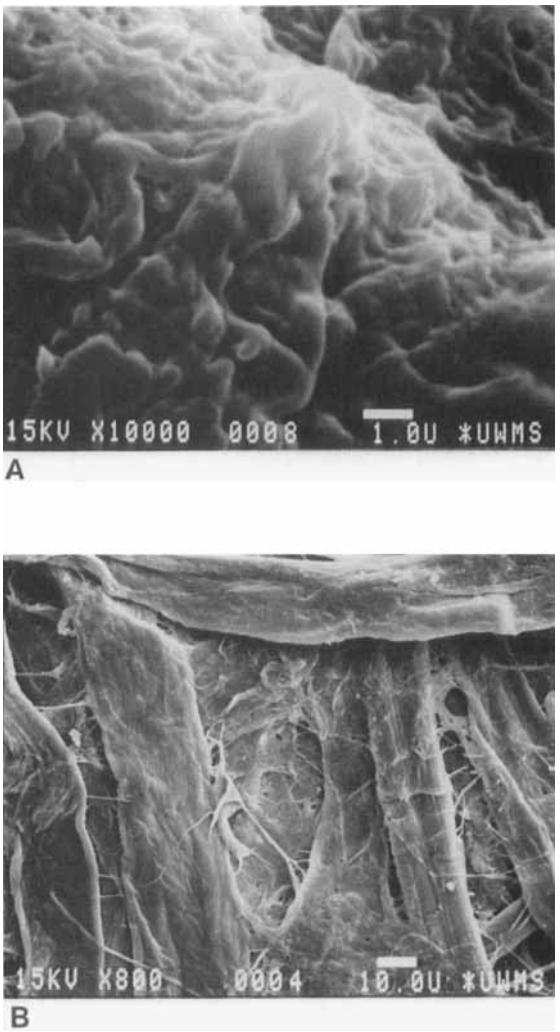

FIG. 26. Scanning electron micrographs of $SiCl_4$-plasma-treated SP at $\times 800$ (a) and $\times 10{,}000$ (b) magnifications.

pressure, lower power, and/or longer treatment times led to the lowest contact angle values. X-ray photoelectron spectroscopy indicated substantial oxygen incorporation with the formation of carbonyl functionalities at the surface of the paper. The oxygen plasma-treated SP was found to perform equal or superior to the control in print screening tests. These tests involved crumple and caustic soda soak evaluation.

Silicon tetrachloride plasmas have a more complex influence on the contact angle values. Because of the multitude and relative ratios of the plasma species resulting from $SiCl_4$ fragmentation, and because of the competition between the silicon-based cations (responsible for hydrophylic functionalities) and chlorine anions (responsible for hydrophobic functionalities) and free radical and excited

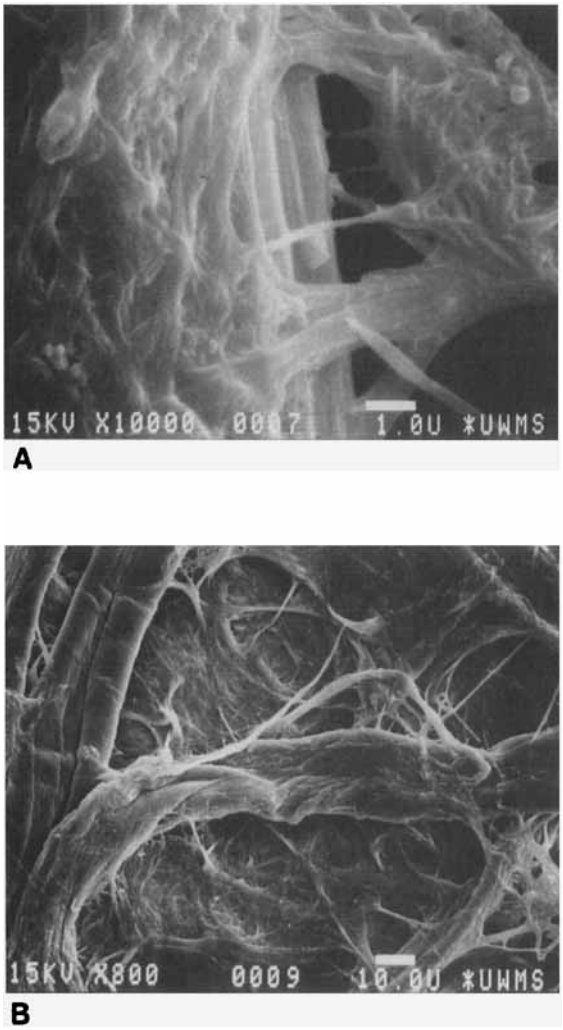

FIG. 27. Scanning electron micrographs of oxygen-plasma-treated SP at ×800 (a) and ×10,000 (b) magnifications.

species, the plots of the contact angles of the surfaces exhibit a significant curvature. Moderate plasma conditions lead to the lowest contact angle values. ESCA data indicate that Si, Cl, and O atoms are incorporated into the surface layers of plasma-treated samples. Postplasma hydrolysis of Si—Cl linkages to Si—OH groups under open laboratory conditions is suggested to be responsible for the oxygen incorporation. The surface atomic composition is correlated with the contact angle values; that is higher oxygen and/or silicon content leads to reduced contact angle.

Carbon tetrafluoride plasmas lead to high contact angle values as a result of intense surface fluorination reactions. The minimal contact angle value in this case was 99.6° under plasma conditions of 115 mT, 61W, and 20 seconds. The intense

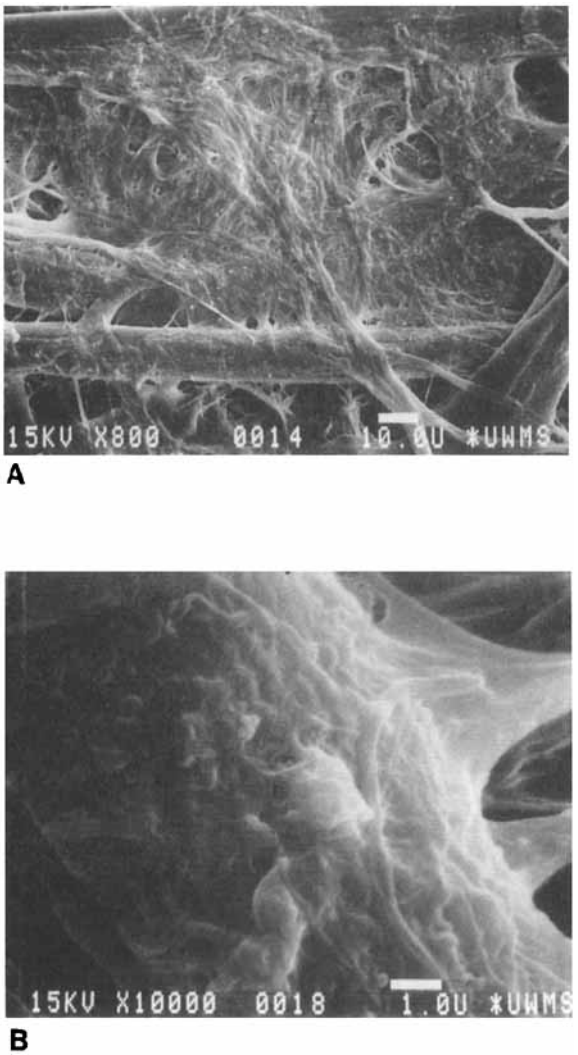

FIG. 28. Scanning electron micrographs of CF_4-plasma-treated SP at $\times 800$ (a) and $\times 10{,}000$ (b) magnifications.

surface fluorination reactions developed during the plasma treatment explain the presence of the elevated contact angle values. The greater surface roughness for all plasma-treated samples, in comparison to sized-untreated substrates, indicates the presence of higher specific surface areas for the treated samples. This characteristic, in addition to the newly acquired chemical surface functionality, influences the surface adhesion behavior of the plasma-treated papers. Because the different plasmas create different functionalities and levels of surface roughness, it is not easy to establish the predominant mechanism for improved adhesion. The possible presence

TABLE 6. Print Screening of Treated Security Paper

Sample identification	Description	Crumple (16×)[a] Face	Crumple (16×)[a] Back	NaOH soak
4566-1	Load 1602 (control)	6	6	Equal to standard
4566-2	Load 1602, oxygen plasma #1	6	6	Better than standard
4566-3	Load 1602, oxygen plasma #2	6	6	Equal to standard
4566-4	Load 1602, $SiCl_4$ plasma #1	4	3	Equal to standard
4566-5	Load 1602, $SiCl_4$ plasma #2	4	4	Better than standard

[a]Rating scale (0 to 6) with 6 = excellent.

of unsaturated bonds and trapped free radicals in the discharge-modified surface layers makes interpretations even more difficult.

Optimum surface modification of security paper by plasma treatment requires only very short treatment times and low energy consumption, making the process economically feasible. This solvent-free approach also eliminates many technological difficulties associated with wet processing. The very low quantity of plasma gases required in addition to the above-mentioned advantages suggest the possibility for the development of a cost-effective process.

In summary, the low contact angle values obtained by oxygen and silicon tetrachloride plasma treatment of unsized security paper samples indicates new possibilities for eliminating or modifying the sizing steps in security paper manufacturing technology.

ACKNOWLEDGMENT

Support for this work is gratefully acknowledged from the National Science Foundation under Grant EEC-872/545.

REFERENCES

[1] D. J. Gardner, N. C. Generella, D. W. Gunnells, and M. P. Wolcott, *Langmuir, 7*, 2498–2502 (1991).
[2] P. Luner and M. Sandell, *J. Polym. Sci., Part C, 28*, 115–142 (1969).
[3] R. A. Young, *Wood Fiber Sci., 8*, 120 (1976).
[4] R. A. Young, in *Cellulose: Structure, Modification and Hydialysis* (R. A. Young and R. M. Rowell, Eds.), Wiley-Interscience, New York, 1986, pp. 91–128.
[5] K. T. Hodgson and J. C. Berg, *Wood Fiber Sci., 20*(1), 3–17 (1988).
[6] J. Borch, *Tappi, 65*(2), 72–73 (1982).

[7] N. Triantafillopoulos, J. Rosinski, and J. Stefano, "The Role of Ink and Paper Chemistry in Water-Based Publication Gravure," in *IPGAC Proceedings*, TAPPI Press, Atlanta, Georgia, 1992.
[8] F. M. Etzler, J. F. Bobalek, and M. A. Weiss, *Tech. Assoc. Graphic Arts*, p. 591 (1993); Paper Presented at 45th Annual TAGA Conference, Minneapolis, Minnesota, April 25–28, 1993.
[9] H. Yasuda, *Plasma Polymerization*, Academic Press, New York, 1985.
[10] R. d'Agostino (Ed.), *Plasma Deposition Treatment and Etching of Polymers*, Academic Press, New York, 1990.
[11] H. V. Boenig, *Plasma Science & Technology*, Cornell University Press, Ithaca, New York, 1982.
[12] H. Biederman and Y. Osada, *Plasma Technology, 3, Plasma Polymerization Processes*, Elsevier, Amsterdam, 1992.
[13] M. Shen (Ed.), *Plasma Chemistry of Polymer*, Dekker, New York, 1976.
[14] D. T. Clark, A. Dilks, and D. Shuttleworth, "The Application of Plasmas to the Synthesis and Surface Modification of Polymers," in *Polymer Surfaces* (D. T. Clark and W. J. Feast, Eds.), Wiley, New York, 1978, Chapter 9.
[15] J. R. Hollahan and A. T. Bell, *Techniques and Applications of Plasma Chemistry*, Wiley, New York, 1974.
[16] H. Boenig (Ed.), *Advances in Low-Temperature Plasma Chemistry, Technology, Applications*, Vol. 3, Technomic Publishing Company, Lancaster, 1991.
[17] A. E. Pavlath and R. C. Landwehr, "Treatment of Fibrous Materials in Glow Discharge," in *Proceedings of 5th International Symposium*, Zurich, Switzerland, 1979.
[18] K. S. Lee and A. E. Pavlath, *Text. Res. J., 45*(8), 625–629 (1975).
[19] A. E. Pavlath, K. S. Lee, and G. H. Robertson, *Vacuum, 25*, 4 (1975).
[20] A. E. Pavlath and K. S. Lee, "Wool Modification Induced by Low Temperature Glow Discharge," in *Proceedings of 5th Internal Wool Textile Conference*, Vol. III K. Ziegler, Ed.), Aachen, September 2–11, 1975.
[21] T. Wakida, K. Takeda, I. Tanaka, and T. Takagishiii, *Text. Res. J.* (January 1989).
[22] S. Sapieha, C. A. Fergyson, R. P. Beatson, and M. R. Wertheimer, *Plasma Chem. Plasma Process., 9*(2), 225–234 (1989).
[23] R. Liepins and J. Kearney, *J. Appl. Polym. Sci., 15*, 1307 (1971).
[24] A. Bialski, R. St. J. Manley, M. R. Wertheimer, and H. P. Schreiber, *J. Macromol. Sci.—Chem. A10*, 609 (1976).
[25] R. Liepins and H. Yasuda, *J. Appl. Polym. Sci., 15*, 2957 (1971).
[26] G. E. P. Box and N. Draper, *Empirical Model-Building and Response Surface*, Wiley, New York, 1987.
[27] F. Denes, A. M. Sarmadi, C. E. C. A. Hop, and R. A. Young, *J. Appl. Polym. Sci., Appl. Polym. Symp., 54*, 55–75 (1994).
[28] A. M. Sarmadi, T. H. Ying, and F. Denes, *Eur. Polym. J.*, In Press.
[29] T. H. Ying, A. M. Sarmadi, and F. Denes, *J. Appl. Polym. Sci.*, In Press.
[30] F. Denes, A. M. Sarmadi, and R. A. Young, in *Proceedings of 205th American Chemical Society National Meeting*, Denver, Colorado, March 28–April 2, 1993.

[31] F. Denes, R. A. Young, and M. A. Sarmadi, in *Abstracts, 35th International Symposium on Macromolecules*, Akron, Ohio, July 11–15, 1994.
[32] X. Tu, R. A. Young, and F. Denes, *Cellulose, 1*, 87–106 (1994).
[33] Y.-A. Kwon, Ph.D. Thesis, Department of Environment, Textiles and Design, University of Wisconsin-Madison, 1993.
[34] S. J. Wu, *J. Polym. Sci., Part C, 34*, 19 (1971).